IEEE Access
Multidisciplinary ⋮ Rapid Review ⋮ Open Access Journal

Received November 4, 2021, accepted November 12, 2021, date of publication November 30, 2021,
date of current version December 14, 2021.

Digital Object Identifier 10.1109/ACCESS.2021.3131382

A Smart Cell Monitoring System Based on Power Line Communication–Optimization of Instrumentation and Acquisition for Smart Battery Management

TIMOTHY A. VINCENT, BEGUM GULSOY, JONATHAN E. H. SANSOM, AND JAMES MARCO
Cell Instrumentation Team, WMG, University of Warwick, Coventry CV4 7AL, U.K.

Corresponding author: Timothy A. Vincent (t.a.vincent@warwick.ac.uk)

This work was funded by the Engineering and Physical Sciences Research Council (EPSRC), Jaguar Land Rover Limited and WMG, University of Warwick, under the Prosperity Partnership grant R004927.

ABSTRACT Energy density of current generation battery packs is insufficient for next generation electric vehicles nor the electrification of the aerospace industry. Currently, approximately a third of energy density is lost due to ancillary demands (e.g., cooling and instrumentation) within a pack, relative to cell energy density. Smart cells, instrumented cells with sensors and circuitry, offer a means to monitor cell performance (e.g. temperature, voltage, current data). Uniquely here we demonstrate our 21700 cells instrumented with internal thermistor sensing arrays with custom miniature interface circuitry including data acquisition and communication components. This circuitry including a power line communication (PLC) system, enables sensor data to be collected and transmitted to a master controller without requiring additional wiring, and can achieve an excellent <0.005 % message error rate. The control and communication system includes the use of adaptive sampling algorithms (during identified periods of low demand, through temperature and current measurements) the cells transmit data at 0.2 Hz, increasing to 5 Hz (normal operation) or 10 Hz (beyond operating limits). This method was demonstrated via drive cycling and external heating to alert the master controller to abnormal operating conditions (rapidly, to avoid missing key features) while saving 65% volume of data during a 90 minute experiment.

INDEX TERMS Power line communication (PLC), cell instrumentation, cell sensing, temperature monitoring, cell cycling.

I. INTRODUCTION

Battery cells currently deployed in automotive and aerospace applications, when considering monitoring and instrumentation, are essentially passive devices. A standard automotive pack, containing 100s of cells [1], usually includes less than 20 temperature sensors to record operating conditions [2]. The additional cost, complexity and weight associated with installing sensors post cell manufacture [3], as well as the current generation Battery Management Systems (BMS) offering limited sensor inputs, prohibit vehicle manufacturers thoroughly instrumenting packs. Current basic BMS may be limited to perhaps total <20 auxiliary inputs [4], [5]). Understanding performance both during development and in-situ operation is vital. We are targeting a distributed BMS arrangement, where traditionally the BMS communicates to gateways placed on the modules in the pack, which then report on the module voltage, and sensor readings etc [6]. A distributed BMS is preferred for improved manageability, avoiding long cables between modules as well as providing a safe and reliable (without a single point of failure), although is noted as more costly compared to a centralized counterpart [7]. In this work we expand this concept so each cell is instrumented and can independently report to a master controller. This proof-of-concept work demonstrates our communication system with a small module of cells and a single master controller. Equally, we envisage a flexible approach to system architecture. We aim to prove our system can operate at an individual cell level; here our instrumented cells individually report to a central controller;

The associate editor coordinating the review of this manuscript and approving it for publication was Barbara Masini.

in later work, we will expand this to an instrumented module utilizing perhaps two PLC networks, where first a collection of cells (fitted with sensors) report to a central gateway, that then further transmits via a secondary PLC network to the BMS.

A. CELL INSTRUMENTATION

Installation of sensors within a pack is not only limited by physical size of the devices, but also the wiring loom required to interface the sensor with the BMS. Sensors, such as thermocouples, are commonly placed in a handful of locations around a pack (typically less than 20 total sensors), which is likely to be insufficient to detect the failure of a single cell [8]. Inside the pack, the communication loom currently requires isolation from the high voltage bus bars as well as robust shielding (to prevent both physical damage for example during vibration, and noise immunity from the power electronics) [9], [10]. This necessary wiring and the cooling system components, reduce the energy density of battery packs. The advantages of high energy density for lithium ion (li-ion) cells (250 Wh/kg, >500 Wh/l) are reduced to between 150 and 170 Wh/kg at pack level [11].

These energy density levels limit the useful driving range of electric vehicles in the automotive sector, and particularly the penetration of electric aircraft in the aerospace industry - current battery technology does not meet demands in terms of weight, seat capacity, speed and range [12]. To satisfy these demands, the pack energy density needs to double (around 500 Wh/kg), as well as a vast reduction in charging time, to fit typical turnaround times and enable multiple flights per day. Furthermore, the cell life-time must be sufficient to require infrequent servicing or replacement - it is estimated a li-ion battery with a 1,000 cycle life would last for several years of automobile use, but perhaps only 200 days if used in an aircraft making 5 flights per day [11].

To ensure pack longevity and safe operation, the thermal management system must be designed alongside the pack monitoring system, as well as ensuring all cells operate at the required temperature. Non-uniform degradation across cell energy capacity has been found when individual cells are not adequately managed, thereby leading to a greater decay in performance over a shorter period [13].

In this work we demonstrate our solutions to instrument cells, leading towards aiding pack development or potentially in-situ experimentation. We define these as smart cells, formed by equipping cells with sensors and electronic readout circuitry. This article will focus on the need for a communication system with signal processing capability at an individual cell or module level, lessening the load on a central BMS. In our previous work we have shown a proof-of-concept communication and data acquisition system for use with externally instrumented cells [14]. We extend upon this work by showing internally instrumented cells, with processing and data acquisition performed at an individual cell level.

B. POWER LINE COMMUNICATION (PLC)

In environments where dedicated communication wiring is not desired (perhaps in remote locations, or space constrained applications), PLC offers an excellent solution to provide communications via existing power line infrastructure. Our previous studies have successfully shown that PLC is suitable for use with li-ion cells in a small module configuration [14], [15]. PLC is of particular interest inside a vehicle battery pack, as it does not suffer from environmental challenges affecting wireless networks, for example: signal attenuation due to objects blocking the signal path; performance degradation due to the need for the system to be contained within a structure consisting of a material with poor signal penetration properties [16]. Utilizing only a physical wired connection removes the possibility of remote access to the network (unauthorized access poses a security risk), an area of concern for vehicle manufacturers, where the network could be carrying safety critical data [17].

PLC has already been identified as a potential solution to reduce the size of vehicle wiring looms, for example in the automotive and maritime industries [18], citing clear cost and weight saving. For automotive use, peripherals in the vehicle may need locating at the extremities of the chassis. This could include items such as a sunroof, electric mirrors or cameras (reversing, side view etc.) [19]–[21]. Video streaming has been demonstrated for in-vehicle use via PLC, highlighting the flexible nature of the protocol, compared to existing low-speed and high reliability serial buses (e.g. LIN–local interconnect network - or CAN – controller area network) [20], [21].

PLC has also been tested at small module levels, involving less than 30 cells in parallel and series configurations of cells (li-ion, of similar format to those integrated in automotive packs) [22]–[24]. These tests, summarized in Table 1, only report over a short term, and perhaps only the order of only a few 1000s of bytes. Sometimes they are also limited to only a single transmission-direction. Such tests fail to demonstrate real-time data acquisition and signal processing, ready for transmission over a period of at least 10s of hours of operation.

In our work we demonstrate the process of sampling instrumented cells, processing the data in preparation for PLC, and then transmitting the data. We demonstrate this can be performed with a collection of 4 slave modems (4 cells) and 1 master receiver, expanding upon the previous work in the literature, testing only a single slave board [22], [24], which avoids the complexity of managing multiple slave devices. In our work these slave devices can generate priority-based interrupts upon the occurrence of designated conditions.

Table 1 further includes other practical experiments found in the literature regarding low voltage PLC towards in-vehicle applications. Li-ion 18650 cells have previously been studied with PLC, although in limited module sizes (6 cells [22], and 30 cells [24]). These studies do not address the challenge of the varying voltage range of the module as the cells are

TABLE 1. Comparable in-vehicle PLC network previous works.

Experiment Aim	Overview of PLC Parameters	Summary of Findings	Reference
PLC proof-of-concept designed towards in-pack deployment, with six 18650 cells, connected serially.	Custom PLC modem, amplitude shift keying (ASK), 7 MHz center frequency.	1,000 packet experiment, zero bit errors. Measurement data collected: internal microcontroller temperature, cell voltage, test potentiometer voltage, check byte. 1 slave/1 master tested in the system. No details of cell voltages nor cycling.	Landinger et al., [22]
Evaluation of PLC modem, with noise sources replicated.	Yamar SIG60 modem, compared against custom PLC modem (direct sequence spread spectrum, DSSS), both 6.5 MHz center frequency.	Packet error rate compared with simulated data, with 1 battery and 1 pair of modems. DSSS modem performance favorable when powerline subjected to Gaussian and single tone noise. No details of cell voltages nor cycling.	Brandl et al., [19]
PLC with 2 and 4 cells in series. Signal waveforms presented.	Cypress PSOC 5lp modems, frequency shift keying (FSK) preferred, 20 MHz frequency.	Single message transmitted between 2 slave modems and 1 master. 20 MHz waveform used to verify communication integrity. No details of cell voltages nor cycling.	Saleem, [23]
In-vehicle PLC system at low DC voltage, e.g. feasibility of PLC with rear camera.	Qualcomm QCA6410 modem, with ethernet interface.	Data (camera video) transmitted via PLC in-vehicle. Use of PLC system restricted to outside battery pack (fixed 12 V DC operation tested).	Hu et al., [21, 26]
Functionality of PLC system with ~thirty 18650 cells (3P10S) tested.	Custom PLC modem, operating with center frequency 10 MHz.	Data generated via FPGA, transmitted via PLC. 18 bits of data decoded. No details of cell voltages nor cycling.	Talie et al., [24]
Replacement of CAN wiring with solely PLC, tested with four cells.	Custom PLC modem, operating at center frequency of 3 MHz.	Demonstration of CAN messages sent via PLC. No further analysis of error rates, nor cell voltages/cycling.	Jousse et al., [25]
Proof-of-concept demonstrating PLC with 4S2P cells; sensor data transmitted and evaluated.	Yamar SIG60 modem, 6.5 MHz center frequency.	Minimal bit error rate achieved (0 %) when transmitting sensor data (external temperature, current and voltage) via PLC, with cells cycled 50 % to 100 % SoC.	Our previous work [14, 15].
Further study demonstrating optimization of PLC bandwidth and greater instrumentation capabilities with 2S2P cells.	TI THVD8000 modem, 5 MHz OOK.	Demonstration of low bit errors achieved when cells cycled. Cells are internally instrumented (temperature), with data sampled at an adaptable rate (temperature, voltage and current sensors). Polling based and interrupt based transmission techniques are evaluated.	This work.

charged and discharged (cycled). Other studies have also included limited 12 V or lower battery cells, [19] and [25], without providing sufficient details on the type of cells tested, nor voltage range. Vehicular PLC can also include replacing wiring outside of the battery pack, although these systems operate at a stable low voltage (12 V DC [26]) network, and avoid the variable voltage found when cycling the battery pack, and need for scalability (to include tens of nodes).

From the studies listed in Table 1, none collect instrumented cell data, and instead collect data from simulated instruments or basic external sensor data (voltage or potentiometer readings). This avoids the complexities involved with sampling sensor data at an adaptable rate, and powering the sensors from individual nodes.

The impedance of a given li-ion cell across the frequency range of interest for PLC is not well understood. The fundamental operation and construction of cylindrical Li-ion cells has been well documented, for example [27]. However, without standard pack layouts (i.e. the configuration of series/parallel cells) and proprietary manufacturing processes and materials used in current commercial batteries, has led to variation in their impedance characteristics. In general, frequency spectrum data is used to understand cell performance, however impedance data is not routinely reported above 10 kHz (for example for use in EIS, Electrochemical Impedance Spectroscopy) [28]. Several studies have been performed analyzing frequencies for PLC, starting at the low MHz range [29]–[32]. The channels available to transmit data via vehicular bus bars were studied by Sabir *et al.* [30]. The cells were mathematically constructed through software modelling packages (e.g. High Frequency Simulation Software. Ansys). It was noted the results were inconclusive, as in some cases modelling does not accurately reassemble practical experiments. In this research field, there is general agreement that frequencies in the range of 1 to 300 MHz will be suitable for PLC (perhaps in the range of 2 to 30 MHz for low-bandwidth [33]) [31], [34], [35]. These studies explain the fundamentals of PLC with cells, although impedance profiles are noted to vary, depending on the construction of the cells tested. In this work, we selected 5 MHz, the highest frequency available with our selected PLC modem, which provides a balanced solution for channel availability; this frequency avoids attenuation due to the cell impedances (low kHz), and switching frequencies of transistors etc. in the 100s of kHz to 3 MHz range [36]. Operating in the low MHz minimizes power consumption compared to higher-bandwidth, higher-frequency alternative modems. In future work we aim to analyze the frequency impedance spectrum for the 2S2P module under test, and to better understand the operation of our PLC network.

Vehicular PLC is not a mature technology, and thus standards for use in vehicles are in their infancy [37].

This provides an opportunity for vehicle manufacturers to develop custom protocols/firmware to meet their pack configuration, where it is already common for manufacturers to define their own modules configurations and instrumentation [38]. In this work the benefits of smart cells are highlighted, where our PLC network can be adapted to handle a near unrestricted number of nodes. Sampling procedures are implemented to optimize the use of available bandwidth (using low bandwidth, less than 1 mbit/s system, but also considering expansion to hundreds of cells). This is achieved while maintaining the benefits of gathering data in high resolution and high spatial detail at an individual cell level, but without the need to burden the BMS with intensive processing tasks.

This also demonstrates the reliable bi-directional communication possible with our PLC network, while permitting interrupt signals to be generated by the slave nodes to send a command to the master BMS, or vice versa.

In this article we detail the results of our practical PLC experiments, demonstrating operation with a 2S2P -2 series, 2 parallel - module (21700 cells); we have structured our article as follows. In the next section we discuss the motivation for instrumentation to be added to passive cells (e.g. in our work we have adapted commercial cells to become smart cells, while maintaining their existing high energy density). In the Methodology section we show our experimental setup and highlight our instrumentation process. Here we concentrate on the practical experimentation to verify our PLC network, and aim to further investigate the operation of our communication system via a model to be developed in further work.

We then present the successful results of our PLC trials, verifying smart cell operation during normal operation and under abnormal conditions (i.e. heated environment to 45 °C, limit of cell recommended operation). This work forms a further proof of concept for PLC equipped smart cells; in the Conclusion we summarize our findings, and then briefly introduce the next stages of our work.

II. MOTIVATION

It has been acknowledged that the current generation BMS lack sufficient measurement parameters to provide advanced warning of a failure modes such as thermal runaway [39]. Blanket measurements of temperature and voltage (i.e. single sensors collect data from a group of cells) reduce the capability of the BMS to monitor abnormal events; in the worst case this is highlighted when the cause or individual cell responsible for triggering a thermal runaway event cannot be identified, even after the event [40].

This issue raises two factors, (i) firstly the lack of sensors to acquire the data, and secondly (ii) the need to capture and store sufficient data within the BMS for analysis (during or post-operation). Gaining detailed information from a cell, addressing (i), has previously been studied; particularly capturing the location of hot spots via thorough temperature sensing (e.g. distributed fiber optics [41], or miniature thermocouples [42]). Also in our previous work, we have shown thermistors along with miniature current and voltage sensors can create datasets to aid understanding of cell operation and future pack development [14].

The handling of these datasets, i.e., addressing point (ii), is not usually studied in the literature. Typically acquiring temperature data at high resolution and frequency can create datasets with file sizes that are unrealistic to process during real-time operation, for example file sizes >1 GB can be expected when capturing distributed fiber optic temperature data at 10 Hz, 0.65 mm spatial resolution, over just a 30 minute period [43]. This problem is lessened at lower spatial resolutions, although we aim to reduce the trade-off between data resolution and available processing time.

We propose our smart cells can capture and pre-process data at an individual cell level. Full resolution (i.e. in the case of our thermistor arrays, 10 mm spatial data with 16-bit ADC readout) can be captured by an interface circuit (sampling frequency limited only by ADC capability). This data ensures detailed analysis can be performed rapidly, without imposing unrealistic loading conditions on the BMS. To construct an overview of the pack performance, key data points (e.g. coolest and hottest temperatures and their locations) can be transmitted back to the BMS.

In previous work our PLC solution, reported with 8 cells 4S2P [14], relied upon polling cells for data, thereby limiting scalability without sacrificing polling rate. The trade-off is between the volume of data collected and the time between sampling sensors for a given cell – assuming the system polls cells in a set order via a loop. This delay is not discussed in existing vehicular PLC articles in the literature, nor is the typical polling methodology discussed [23], [31], [44].

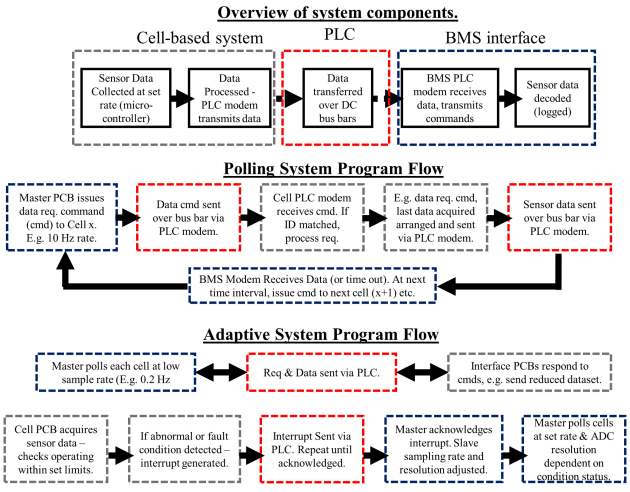

FIGURE 1. Block diagram comparing operation of polling system with our interrupt based network.

In this work we demonstrate a lower polling rate can be implemented during cell resting (idle, no current demand or temperature increase). Immediate higher sampling rates can be reinstated by generation of an interrupt (block diagram shown in Fig. 1). This demonstrates the effective

TABLE 2. Overview of study objectives.

Objective	Study	Method	Success Indicator
(i)	Reliability of PLC	Verify PLC performance against known standard (e.g. CAN).	Experiment demonstrating equal performance (reliability, transmission time) to wired communications, over a period of 100 hours. Demonstrate minimal errors (<0.1 %) and low power consumption (<200 mW).
(ii)	System Bandwidth	Transmit high resolution (16 bit) ADC data via PLC for all four cells.	Transmit data at sufficient sampling rate (i.e. set to 10 Hz) and 16-bit resolution to capture transient (drive cycle) profile. Success determined by low error rate, and sufficient data received to determine peak current draws/temperature values during experimentation (compared to reference cycler or external sensors).
(iii)	Bi-directional Communication	Transmission of data from cells to master (normal polling operation). Transmission of commands from master to cells and interrupts from cells to master. Interrupts should enable faster means of monitoring cells without waiting for polling to loop around.	All experimentation will include logging of data received via PLC. Adaptive sampling (during e.g. drive cycle or when exposed to external heating) will demonstrate ability of cells to generate interrupts. Success determined if each of the four cells can be independently sampled at appropriate (perhaps different) adaptable rates and urgently communicate with master.

bi-directional communication; during rest operation, the polling signal is sent from the master to each slave modem; however, upon occurrence of an alert condition (current demand or temperature increase), the interrupt command is sent from triggered slave board to master.

To enable the system to function correctly in this work, when utilizing only a single communication channel/ frequency, the master dictates the sampling rate for each individual cell (selected via status report or alert from cell).

The slave cells must be aware of the usage of the PLC channel, where in our current system, data is discriminated only by the time domain (frequency division is an option considered for future work) – data transmissions must currently not overlap or risk corruption.

PLC also offers benefits regarding a fully integrated and connected pack. Signal integrity and strength in this work was maintained regardless of cell location, mitigating concerns of wireless technologies and reception strength dependent on path between transmitter and receiver (the channel is likely to be blocked and signal attenuated over short distance by metallic materials used in construction of pack, i.e. not least aluminum cell cans) [16]. In additional to security risk, miniaturization of antennas suitable for communication within a pack, whilst maintaining signal integrity, is still a challenge for a wireless BMS [45].

Furthermore, with bi-directional modems, messages can be received between slave devices. Inter-slave messages are discarded in this work, but in the future could be used to verify operation of neighboring cells, without requiring the intervention of the BMS.

III. METHODOLOGY

The PLC system developed in this work is demonstrated with li-ion cells (21700 format, 5 Ah capacity, model and manufacturer are not disclosed). Due to the business confidential nature of our work we are not able to provide raw data files, and can only present the plots shown in this work.

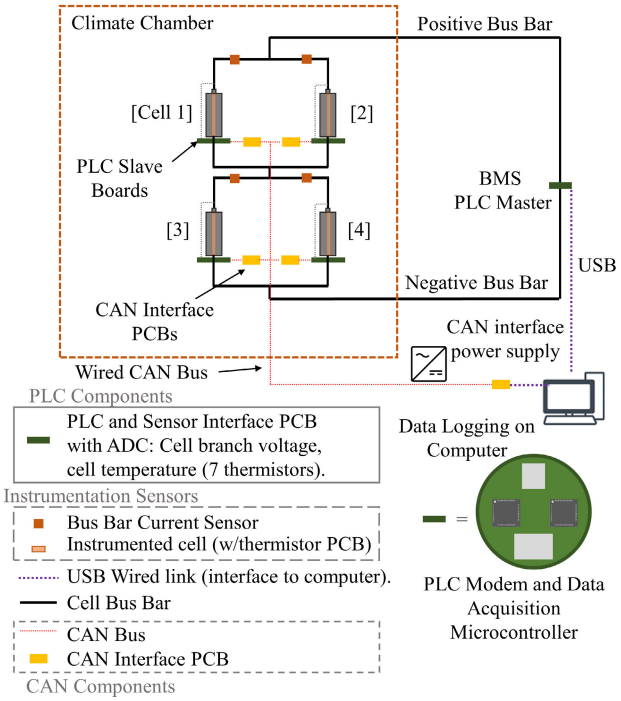

FIGURE 2. Schematic of instrumented cell configuration.

To demonstrate the functionality of the PLC system, a 2S2P arrangement of cells was selected (4 cells total); this demonstrates functionality with a 5 node network (4 slaves, 1 master), which could form a building block for expansion into larger module concepts. The interface PCB, with a compact design, can currently fit on top of a 21700 cell can. It is proposed this system can be adapted to fit other cell types, and integrated into modules. The following objectives were targeted, as summarized in Table 2.

A. SYSTEM OUTLINE

The 2S2P arrangement results in a 10 Ah module with a maximum voltage 8.4 V. Each cell is instrumented with internal

temperature, voltage and current (bus bar mounted) sensors, as shown in Fig. 2. All experimentation was performed within a climatic chamber, maintained at 25 °C. During each cycling experiment, sensor data were transmitted over PLC (i.e. at the 10 Hz standard configuration, from each cell or at a variable rate, shown in Table 3). To provide reference data, messages were also sent via USB and CAN, connected via dedicated wired connections.

The implementation of our PLC network enables each cell to communicate via its existing terminals, without additional wiring. The CAN bus requires cabling for power and communication, which increases the necessary wiring harness around the module and interconnections. In this design the PLC boards are configured to minimize wiring between cells (1 modem per cell), although this design could be reconfigured for a group of cells to share an interface board, as demonstrated in our previous work [14]. The interface board acquires data from the sensors; firmware then transmits the data by the three medium (USB, PLC and CAN).

B. PLC AND INTERFACE BOARD DESIGN

A small, 20 mm diameter, PCB was designed and manufactured to contain the interface acquisition components and data transmission (PLC and USB, with expansion wiring for external CAN interface) circuitry. Photographs, Fig. 3 (a) and (b) label key components. In its current form, the PCB can be fitted on top of a 21700 aluminum can; concept photographs with rapid prototyped enclosure are shown in Fig. 3 (c) and (d). The enclosure housed the circuitry in the correct location, but later designs need to be constructed using a flexible and less-brittle plastic material. The enclosure screws into a standard M2.5 thread in the can, formed as described in our instrumentation process below, and a flexible thermistor PCB is inserted into the cavity at the core of the cell. In this initial study, the PCB is mounted separately away from the cell, with alternative fittings installed.

We have previously demonstrated PLC enables reliable networks to be formed in a small module using low bandwidth modems [14].

The PLC modem (i) employed was a Texas Instruments (TI, USA) THVD8000DDFR [46]. The small outline transistor (SOT23, 8 pin) package offered a small size (2.9 × 1.6 mm), and the modem was available at low cost (<$3, even at relative low volume of 1,000 pieces) and operates at low voltage (3.0 to 5.5 V). This modem offers an order of magnitude improvement in bandwidth beyond our previous iteration (now permitted up to 500 kbit/s), although this is generally still classed as a low bandwidth modem (less than 1 mbit/s). This class is preferred for our work, where the devices are solely battery powered. Thus, capability must be balanced with power consumption. This IC required few external components (only needing typical capacitors to extract high frequency component, and a resistor to set operation frequency).

ADC (iii) – TI ADS114S08 was selected to offer high resolution (16 bit) and high precision (buffered inputs,

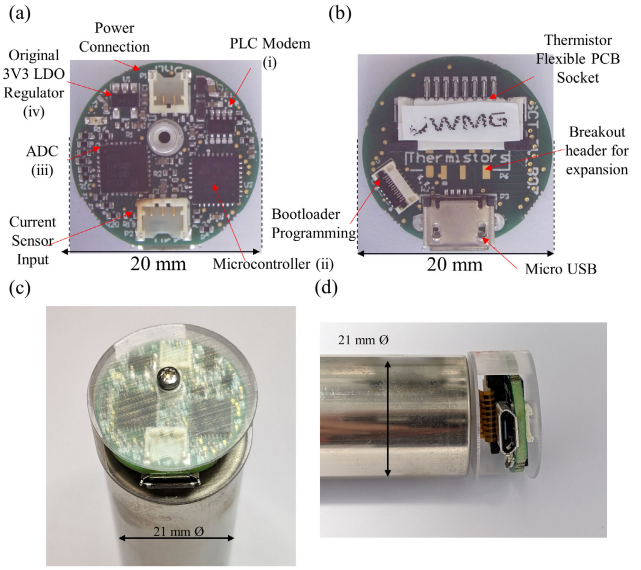

FIGURE 3. Photographs of interface and PLC PCB; (a) top view of 20 mm PCB, key components labelled, (b) bottom view of PCB, headers implemented for laboratory experimentation (USB, CAN breakout). PCB compact size enables installation on 21700 cell, top view (c) and side view (d).

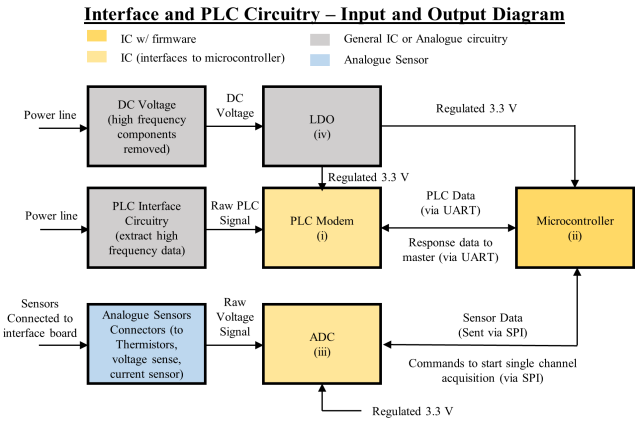

FIGURE 4. Block diagram of major components on interface and PLC PCB, general flow and input and outputs shown.

to compensate for variation in thermistor resistance, i.e. this variation, their measurement principle, can load ADC inputs with a nominal input impedance of 10 kΩ). This IC is available in a compact package (QFN32), enabling up to 12 input channels (9 required, 7x thermistor inputs, 1x voltage reading, 1x current reading). There is additional capacity to enable a larger array of thermistors to be constructed or expansion for other sensors (e.g. pressure or gas).

Microcontroller (ii) – ATSAMD21E18A (Microchip, USA). A compact IC was required (QFN32), without limiting connectivity nor capability (48 MHz clock speed, enabling real-time calculations and basic signal processing to be performed without needing transmission to the master). In terms of input and output requirements, SPI and UART are needed for sensor and PLC modem connectivity, respectively. I2C is desirable for future work, where many miniature sensors may

offer I2C connection options. This microcontroller requires minimal external components (an external crystal is not required).

LDO Voltage Regulator (iv) (low-dropout) – TI TPS73133. A LDO regulator is preferred, offering a very stable output voltage (this model found to be reliable, with minimal approximately 0.010 V dropout) and low noise (considering analogue circuitry for thermistors). A buck boost regulator was trialed, but found to increase switching noise in the circuit, and reduce regulation efficiency. This limits our operation range in this work (around 3.3 to 4.2 V only).

Total power consumption was noted to be less than 100 mW (4.0 V power supply), during normal operation but including a power indicator LED (as tested); power consumption without this LED is approximately 48 mW. Total peak power consumption during experiment transmission was around 150 mW.

The TI PLC modem selected also offers flexible data input; data is transmitted over the power line via on-off keying (OOK) modulation and demodulation. The modem accepts a digital signal encoded via OOK; typically RS-485 would be suitable, offering data transfer speeds up to 500 kbit/s, considering operating at 5 MHz, 10 cycles per bit recommended for robustness [46]. In this work, the RS-232 protocol was selected for simple integration with the ATSAMD21E18A microcontroller, without requiring further ICs; however its speed was limited to the maximum baud rate on the microcontroller (115.2 kbps). It is proposed this rate could be increase via software and in future work we aim to test the maximum bit rate at 5 MHz, and attempt multiplexing via a separate frequency transmission.

For these experiments, precise temperature data at key points during testing is desired, thus full ADC resolution (16-bit) was selected from all 4 cells, for all sensors. With the board ID (2 bytes), status indicator (1 byte), 9 channels of sensor data (18 bytes together), timestamp (4 bytes) – in total each board will send up to a 25 byte reply to each data request.

The operation of the LDO is limited to 3.3 V, thus in this work the state of charge (SoC) of the cells is maintained above 50 %. In preliminary tests, a buck boost regulator was trialed, however potentially increased power consumption by around 50 %. In future work we aim utilize a LDO (operating at around 2.5 V) to enable limited operation at lowest SoC (2.5 V) – where the microcontroller is listed by the manufacturer, as functional to 1.62 V- offering a standby mode. By triggering the device awake, a buck boost regulator would be suitable to power remaining components (to permit full operation) needing a 3.3 V supply.

C. REFERENCE COMMUNICATION

The PLC system relies only on the bus bars for data transfer – to verify the system's operation, the received data was compared to reference values transmitted via USB (microcontroller equipped with USB interface) and CAN (an external CAN modem was installed via an SPI link. Unlike the PLC system used here, CAN buses are designed to operate with a common ground connection. As each smart cell powers a dedicated interface board, 'ground' here is relative to the negative terminal on the cell. Isolation circuitry is needed to separate the signal grounds (SPI ground separate from CAN bus). A CAN controller (MCP2518FD, Microchip, USA) was selected, for flexible data rate (FD) capability. This enables longer messages to be transmitted via the bus (64 byte limit, compared to 8 bytes) [47]. Therefore, identical messages can be transmitted via both PLC, USB and CAN bus which are up to 25 bytes length.

It is noted CAN-FD offers improved message handling, but not necessarily higher transmission rates; sometimes to require backwards compatibility 500 kbps is utilized (ringing can occur at higher data transfer rates); however newer devices (with ringing suppression) have enabled CAN-FD to be specified for data transfer up to 5 mbps [47]. In this experimental setup, power is required separately for the CAN bus and controller circuitry. In total this circuitry alone required 220 mW per board (operated at 5.0 V).

Reference data was also gathered via a standard USB connection. In this work these data were not needed for comparison, although could be utilized in the future to better analyze PLC performance (e.g. potential time delay via PLC). The typical maximum baud rate for microcontroller USB (UART) to computer is 115.2 kbps. The maximum message length (reportedly 64 bytes [48]) was not found to be exceed in this work.

D. SENSOR DEVELOPMENT

The ADC was directly used to measure cell voltage, although in future work this could be extended to provide a reference electrode capability in which the individual anode and cathode voltages are measured within a modified cell, thus offering insight into the individual cathode and anode potentials. In terms of current and temperature sensing, custom circuitry was developed to optimize a Hall Effect current sensor (ACS37612, Allegro Microsystems, USA) and an array of thermistors (NCP03WF104F05RL, Murata Manufacturing, Japan) to operate with each cylindrical cell.

Cell internal resistance should be minimized during design, to reduce self-heating and reducing power capability, as well as kept consistent between cells, to minimize aging through mismatched parallel cells [49]. To sense current, through each individual cell a Hall Effect sensor was chosen to detect the magnetic field changes from a conductor, without requiring a series connection. In this work the sensor was mounted to the bus bars, Fig. 5 (a), but did not interrupt the cell-to-module connection, thus cell resistance was not affected (not increased nor consistency altered). A shunt resistor current sensor was similarly disregarded.

To sense current, through each individual cell a Hall Effect sensor was chosen to detect the magnetic field changes from a conductor, without requiring a series connection. In this work the sensor was mounted to the bus bars, Fig. 5 (a), but did not interrupt the cell-to-module connection, thus cell

resistance was not affected (not increased nor consistency altered). A shunt resistor current sensor was similarly disregarded.

To optimize the sensitivity of the sensor (generally capable of range of 100+ A), a notch (4 mm minimum width) was cut into the bus bars, Fig. 5 (b). The top of the sensor was mounted onto the bus bars for best sensitivity. Prior to measurements, the sensor was calibrated using a bench top power supply, with resistive loads connected in series (1, 2 and 5 Ω) to pass various currents through the bus bar. The bus bar was flipped during calibration, to test current flow in either charge or discharge direction.

To ensure the current sensor was not affected by bus bar voltage, the supply voltage was varied (3.3 to 4.2 V), which was also used to calibrate the ADC readings.

Temperature gradients are likely to be formed along cylindrical cells due to non-uniform cooling (such as tab vs radial) and variations in thermal conductivity from the cell core to the tabs and surface [50]. These gradients should be minimized, else risk premature aging of the cells. To aid cooling system design by providing data of core temperatures along the length of the cylindrical cells, an array of thermistors was designed, mounted on a flexible PCB. Each PCB contains 7 sensors, spaced at 10 mm distances; the schematic is shown in Fig. 6 (a). This array is then inserted into the core of the cell.

In this work, the internal thermistor sensors will be referred to via the notation 'S#' where '#' will be their identification number marked on the figure. Similarly, external sensors will be labelled as 'Ext_S#'. The NCP03WF104F05RL thermistor was selected to offer 100 kΩ nominal (25 °C) resistance, thus reducing self-heating inside the cell and minimizing current demand. The miniature size (0201 imperial size, 0.6 mm length) was suitable for insertion into a cell with minimal impact on consuming volume inside the cell, and minimal height (0.3 mm) prevented contacting with the jelly roll.

The sensor calibration process will be detailed in an upcoming article and will therefore not be repeated here; the sensors are calibrated against reference thermocouples in a climatic chamber, with temperature varied between 20 and 50 °C (5 °C steps, 2 hours per step).

The flexible PCBs, Fig. 6 (b), required preparation (protection and rigidity) prior to installation inside the 21700 cells. Previous works have inserted polymer coated PCBs without further coatings into cylindrical cells [51], and although in general these are resilient to the corrosive electrolyte, the sensor positioning inside the cell is not repeatable.

In our process, the sensor arrays are fully prepared prior to installation in the cells (i.e. which must be performed in an oxygen and moisture free environment), which entails a repeatable sensor array layout. Our sensor arrays are covered with chemical resistive heat shrinkable tubing, which completely protects the components from chemical and physical damage (i.e. polymer coatings could easily be removed or breached due to friction during insertion into the cells). The protective tube further aids the rigidity of the boards, which

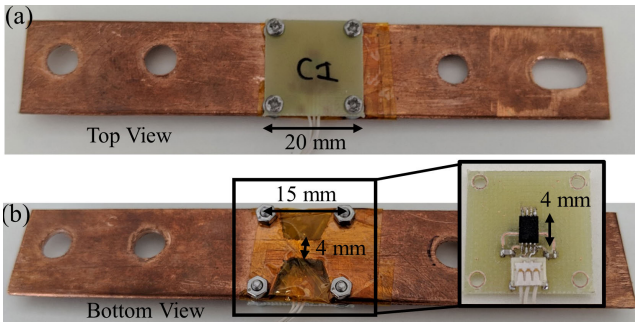

FIGURE 5. Photographs of bus bar mounted current sensor, (a) top view of bus bar prior to installation in rig, (b) bottom view, showing notch cut into bar.

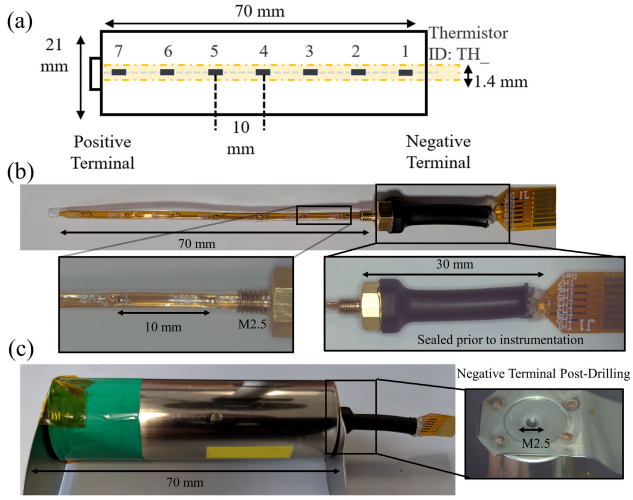

FIGURE 6. Instrumented cell formation, (a) schematic of proposed 7 thermistor temperature sensing array, (b) flexible PCB prepared for instrumentation, (c) completed instrumented cell ready for experimentation.

ensures the sensors are not twisted or bowed when inserted into the cell, while forming a circular shape to equally fit inside the center of the empty mandrel of a cell.

To ensure reproducible insertion and avoid use of adhesives near the cell (i.e. viscous glue used to seal gaps/holes in the can could penetrate into the cell and react with the electrolyte) we have developed a friction drilling process to create an opening in the can for instrumentation. We will detail this process further in a dedicated upcoming article. Briefly, a friction drill bit is used with a mini milling machine to form a 1.6 mm hole in the negative terminal of the can. This process avoids cutting material (potentially creating swarf and metal fragments which could enter the cell), only pushes material to create a hole (thereby maintaining the integrity of the cell and minimizing damage to the negative current collector). The methodology employed for cell preparation and sensor insertion is presented in a dedicated upcoming article and will therefore not be repeated here. The cell modification procedure was performed in an argon glove box, with less than 0.1 ppm moisture and less than 10 ppm O_2.

TABLE 3. Summary of sampling rates and states during adaptive sampling.

State Number (three letter abbreviation)	Sampling Rate	Current Condition	Temperature Condition
0 (NOM -nominal)	0.2 Hz	± 0.5 A from baseline	±5 °c from ambient
1 (ALT - alert)	5 Hz	>0.5 A charge/discharge	> 10 °C and <40 °C
2 (EMG - emergency)	10 Hz	> 10 A charge/discharge *	< 10 °C or >40 °C
3 (ERR -error) *	-	-	-

* - state or condition not experienced during these experiments.

This hole is sufficient to permit M2.5 thread tapping via a thread forming bit (again avoiding cutting material). We have developed sensor fittings based on this M2.5 opening, in the case of this work for thermistor arrays, although potentially a wealth of sensors, provided they could fit through a hole of less than 1.8 mm diameter, could be inserted via this process (variety of temperature sensors, pressure, gas etc.).

By using a thread-based insertion method, this ensures the sensors are securely fixed into the cells. This relates to our target to instrument cells fit for all types of operation (i.e. normal and perhaps abuse operation). The thread enables, if necessary, the sensors to be removed (again, an oxygen free etc., sterile environment is required).

A brass fitting, Fig. 6 (b) with enlarged views, was designed to secure the thermistor array a total of 70 mm into the cell core. Adhesive heat shrink tubing was applied external to the cell (approximately 30 mm length) to affix the fitting to the flexible PCB assembly, and enables accurate positioning of the sensors (z direction) into the can. This seal also prevents electrolyte from penetrating through any gaps the internal opening in the fitting (between the brass material and the flexible PCB).

In this instrumentation procedure, only the cell drilling and the sensor insertion is performed inside this environment. The majority of the sensor assembly detailed above, is performed in a standard laboratory (all component dried for 8 hours in vacuum oven at 40 °C prior to insertion). The completed instrumented cell is shown in Fig. 6 (c).

E. ADAPTIVE SAMPLING

In previous instrumented cell work, such as [42], [52], [53], to the authors' knowledge there have not been reports of adaptable or variable sampling rates according to cell operation. Where standard laboratory equipment is used to log data when independent of a cell cycler (which could correlate i.e. temperature data collection and cycling operation mode), standard fixed data acquisition rates are typically employed. In terms of instrumented cells, equipment separate from the potentiostat is often required. Potentiostats are usually equipped only to sense thermocouples, and are not suitable for interfacing to non-standard sensors (and typically are limited to perhaps 1 sensor per cell). Furthermore, experiments such as testing abuse conditions, may not require a cell cycler. In these scenarios logging data at a fixed rate ensures capturing of every event, but is inefficient, and entails huge (order of several gigabytes of data) can be collected for short experiments (under 24 hours) if high acquisition rates and many sensors (greater than 10) are required.

In this work we demonstrate the ability of our interface circuitry to adapt the transmission rate of data to the master controller. Pre-processing the data at the cell level, ensures features of interest in the data are not lost (due to down sampling or resolution reduction) and removes this processing load from the BMS. Furthermore, this reduces the PLC bandwidth required per cell in the system, enabling faster response to abnormal conditions via cell interrupts (outline of program operation shown in Fig. 1). The sensor acquisition rate within the interface circuitry itself is not reduced (10 Hz), however this can be averaged when required, to reduce the volume of data transmitted over the bus bars. The resolution (16 bit ADC) is also not reduced internally, however lower resolution (8 bit) data is transmitted at the lowest transmission rate. Only 2 temperature readings (hottest and coolest, from the array of 7 sensors) are transmitted (along with their location within the array). This greatly reduces the length of the data content of each message string (now needing only 5 bytes compared to the standard 18).

We have previously reported data logged between 5 and 10 Hz continuously (upcoming article and [14]). In this section of experiments, data are transmitted at a low rate (0.2 Hz), standard rate (5 Hz) or high rate (10 Hz), dependent on the status of each individual cell. During cell rest or low demand conditions (defined current <0.5 A charge or discharge, cell temperature close to ambient defined as a range of 20 to 30 °C) the (default) low rate is employed. During periods of standard operation (cell temperature <40 °C and >10 °C, current >0.5 A, either charge or discharge) data are transmitted at 5 Hz per cell. When the cell temperature exceeds manufacturer recommendations or operates at higher current charge-rates or within more diverse temperature regions (here set at above 40 °C) the higher rate, 10 Hz, is initiated. The three states above and an error state (e.g. faulty sensor or disconnected – not observed in this work) are summarized in Table 3.

To allow correlation between the network of cells, the master controller defines the data transmission rate from each cell. Initially 0.2 Hz sampling rate is set for each cell, but then adapted according to a status value (sent with every cell's data transmission) or an interrupt transmission. This interrupt is sent independently from an individual cell when abnormal conditions detected (immediately once the PLC channel is available). An interrupt is set to only be sent when the channel is available, to avoid corrupting messages via their overlapping (thus a lower nominal-sampling-rate is preferred to ensure maximum availability). To ensure an interrupt is received successfully, and as quickly as possible, the master will prioritize sending a response to the appropriate slave cell. If the slave cell does not receive an acknowledgment to the interrupt within a short period (set here to 100 ms), further interrupts will be generated. This procedure was sufficient for handling the 4 cells in this configuration, although it could be adapted as necessary, to allow scalability.

The parameters defining each status category were selected according to laboratory conditions (climatic chamber 25 °C ambient) and manufacture datasheet recommendation. It is proposed these could be adapted (with voltage, temperature and current sensor data) to be used to refine data transmission rates accordingly. By utilizing an adaptive sampling rate, this demonstrates the development path to a scalable PLC network (reducing time delay introduced by circular polling of cells) and vastly reducing unnecessary data collection and logging by the master (or BMS) during typical cell operation.

F. EXPERIMENTAL SETUP

A cell test rig was designed to safely house the 2S2P instrumented cell layout, with current sensors and reference data collection hardware, Fig. 7 (a). Each cell was fitted with an external thermistor array (USB data logged) and a reference thermocouple (centrally located, SE001, Picolog, UK). An enlarged view of cell 4, Fig. 7 (b), shows the connection to the bus bars/CAN reference interface hardware. The rig is the final assembly of the schematic in Fig. 2.

This test rig was used for the comparative experiments with CAN configuration and drive cycle testing. Reference performance tests (RPTs) were performed on the cells, during which the cells were connected singularly in a test rig, without parallel connections (and without PLC nor CAN connections). Following the RPTs, three types of experiment were performed. Firstly, standard cycling to verify functionality of the PLC network, secondly a transient current profile – devised to analyze sample-rate adaptation via current sensor sampling, and finally external heating of the cell – thereby initiating adaptive sampling rates through temperature sensors readings exceeding standard operating conditions.

G. RPT

To validate the integrity of our instrumented cells a RPT was performed during each stage of the instrumentation process (this process will be discussed in a second dedicated upcoming article). Additionally, after the significant cycling

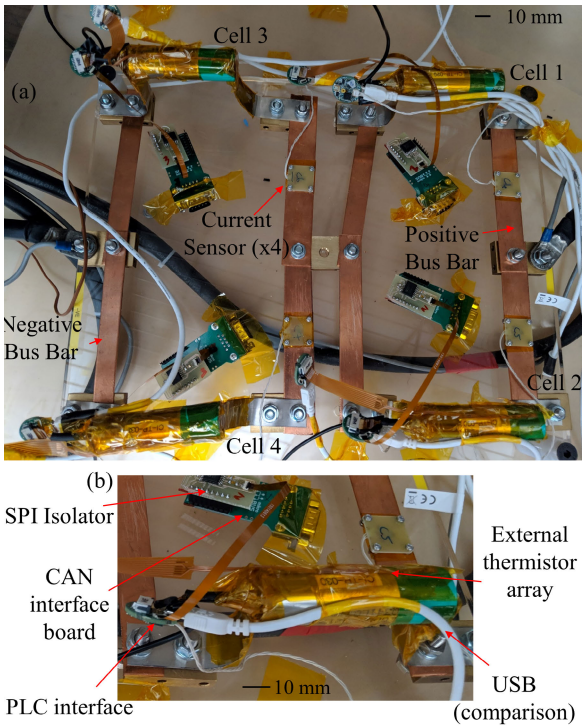

FIGURE 7. Cell experimental rig, (a) photograph of 2S2P layout with current bus bar sensors (CAN bus not connected), (b) enlarged view of instrumented cell showing internal and external sensors.

performed to characterize the PLC network (experiments detailed below, required to assess objectives listed in Table 1), a post-cycling RPT was performed to quantify performance loss over this period. In further work, this will be extended to age the cells over a greater number of cycles.

Full details of the characterization process involved in the RPT will again be discussed in a detailed upcoming article. For complements, the RPT is summarized as follows: the study consists of a full charge and discharge cycle (2.5 to 4.2 V) to observe the energy capacity of the cell. The cell is also characterized via pulse discharge steps. Each RPT lasts just over 24 hrs. These RPTs were performed via a cell cycler (VSP-300, Biologic, France), configured with maximum charge/discharge 10 A (2C), compliance voltage 5 V. Prior to running the RPT, the cell impedance is measured (1 kHz AC analyzer, BT3564, Hioki E.E. Corporation, Japan) to ensure the integral condition of the cell (i.e. no short-circuit risk). The initial RPT studies have been reported in a dedicated article; in this work the fourth RPT (post PLC study) is shown. During this RPT the temperature and current are monitored. PLC is not utilized (to avoid influencing the measurement).

H. PLC VERIFICATION EXPERIMENT

We propose that our PLC network is suitable for communicating with instrumented cells, and can be adapted to meet the specific needs (sampling rate, reliability, message integrity, data resolution etc.) for laboratory and in-situ testing.

TABLE 4. Capacity of cells measured via RPT.

Capacity	Cell 1 [Ah]	Cell 2 [Ah]	Cell 3 [Ah]	Cell 4 [Ah]
RPT 1 (Pristine)	4.830	4.826	4.811	4.826
RPT 2 (Post Drill)	4.803	4.809	4.804	4.813
RPT 3 (Post Instr.)	4.790	4.803	4.795	4.782
RPT 4 (Post Cycling)	4.671	4.687	4.606	4.641
Capacity Fade [Ah] (%)	-0.159 (-3.3 %)	-0.139 (-2.9 %)	-0.205 (-4.2 %)	-0.185 (-3.8 %)

To verify our setup at minimum performs adequately compared to a known standard, a CAN was formed, as commonly used in automotive applications). A test at the maximum sampling rate (10 Hz maximum, defined in Table 2) for all 4 cells was initiated for a period of nearly 100 hours.

A cycle was constructed to vary the cell SoC between 50% and 100 %, consisting of three phases: (i) Pulse discharge stages (similar to RPT, verify operation with transient pulses of current demand); (ii) 10 cycles of C/2 discharge, then C/3 charge (verify PLC operation, monitor cell core temperature during prolonged discharge), (iii) pulse discharge stage repeated. This program was performed on a module cycler (FTV 200-60, Bitrode, USA).

I. DRIVE CYCLE

Following the verification of our PLC configuration, the adaptive sampling routine, implemented via the current sensor measurements detailed in Table 2 'Current Condition', was tested via a drive cycle profile. This transient test, including abrupt periods of charge and discharge pulses, was based on a profile derived from a real vehicle driving within the urban environment in Coventry City, UK [54]. The profile extracted from the EV containing a complete battery system, was scaled by a factor of 10, to conform to the lower capabilities of this single module. Similarly, the Bitrode module cycler was used in this experiment. Periods of reduced and then intense current draw were used to demonstrate the option of lowering sample rates during periods of reduced demand from the cells, and rapidly re-instating faster sampling rates when required (previous work demonstrated this drive profile has minimal impact on cell temperature [14]).

J. CELL TEMPERATURE ADAPTIVE SAMPLING

To demonstrate the ability of the system to respond to temperature changes at an individual cell level, in this trial the external cell temperature is heated to just over 45 °C. In our work we have noted cell temperature is a factor of rate of charge/discharge as well as its duration. Additionally, cell temperature could rise or fall suddenly due to inappropriate cooling or external (or ambient) heating factors. Therefore the cell temperature must also be able to trigger faster data transmission rate when operation exceeds safe limits. Here, the limit of low demand operation is defined as 30 °C, and 40 °C internal temperature to trigger the maximum (10 Hz) sampling rate, defined in Table 2.

To initiate a temperature rise, regardless of current demand, an external heater pad was wrapped around the cell, located towards the positive terminal of the cell. A temperature controller was used to maintain a constant heater pad temperature of 45 °C. In this configuration the external sensors will record higher temperatures throughout, with internal sensors reaching a lower peak temperature. This procedure demonstrates heating the cell above 30 °C (triggering 5 Hz data transmission) and up to approximately 40 °C internal temperature (triggering 10 Hz data transmission), before returning to ambient temperature (25 °C). The experiment was performed on a single cell in open circuit condition, for safety reasons, while inside a climatic chamber, but without a cell cycler required.

IV. RESULTS AND DISCUSSION

A. RPT

A RPT was performed at each stage of the instrumentation process (pristine, post-drilling, post-instrumentation) and finally after post-cycling. The final values ('post-cycling') were measured following 4x RPT studies, around 50x cycles (C/2 discharge, C/3 charge, to 50 % SoC, over approximately a 1 month period) and 5x drive cycle profiles.

The capacity variation, Table 4, and impedance variation, Table 5, are summarized below. The impedance measurements were performed manually (BT3563), with probe attachments. For capacity measurements, a variation of nearly 2 % could be expected as measured in preliminary experiments, due to tolerances (VSP-300 measurement error, variation in connection quality to cycler, etc.).

Capacity fade refers to the degradation found between pristine condition and final post-cycling measurements. Similarly, impedance rise refers to the change in impedance observed over the same period.

Tables 4 and 5 show approximately 3 % degradation (average 3.33 %) is found for cells 1, 2 and 4 during the complete experimental stage. This loss is greater (4.26 %) for cell 3, which correspondingly has a higher resistance measured, greater than 25 mΩ, post cycling, as well as lower initial capacity (4.811 Ah) and higher resistance (initially 24.18 mΩ, all others less than 24 mΩ). This cell data demonstrates the cell is weaker compared to counterpart cells, which could influence longer-term aging of the module [49]. The RPT data (current, voltage, external and internal temperature) is shown for cells 3 and 4 during the final test

TABLE 5. Impedance of cells measured via analyser.

Capacity	Cell 1 [Ah]	Cell 2 [Ah]	Cell 3 [Ah]	Cell 4 [Ah]
RPT 1 (Pristine)	23.67	23.91	24.18	23.74
RPT 2 (Post Drill)	23.69	23.87	24.35	23.94
RPT 3 (Post Instr.)	24.16	24.12	24.69	24.13
RPT 4 (Post Cycling)	24.27	24.39	25.50	24.52
Impedance Rise [mΩ] (%)	0.60 (2.5 %)	0.48 (2.0 %)	1.32 (5.4 %)	0.78 (3.3 %)

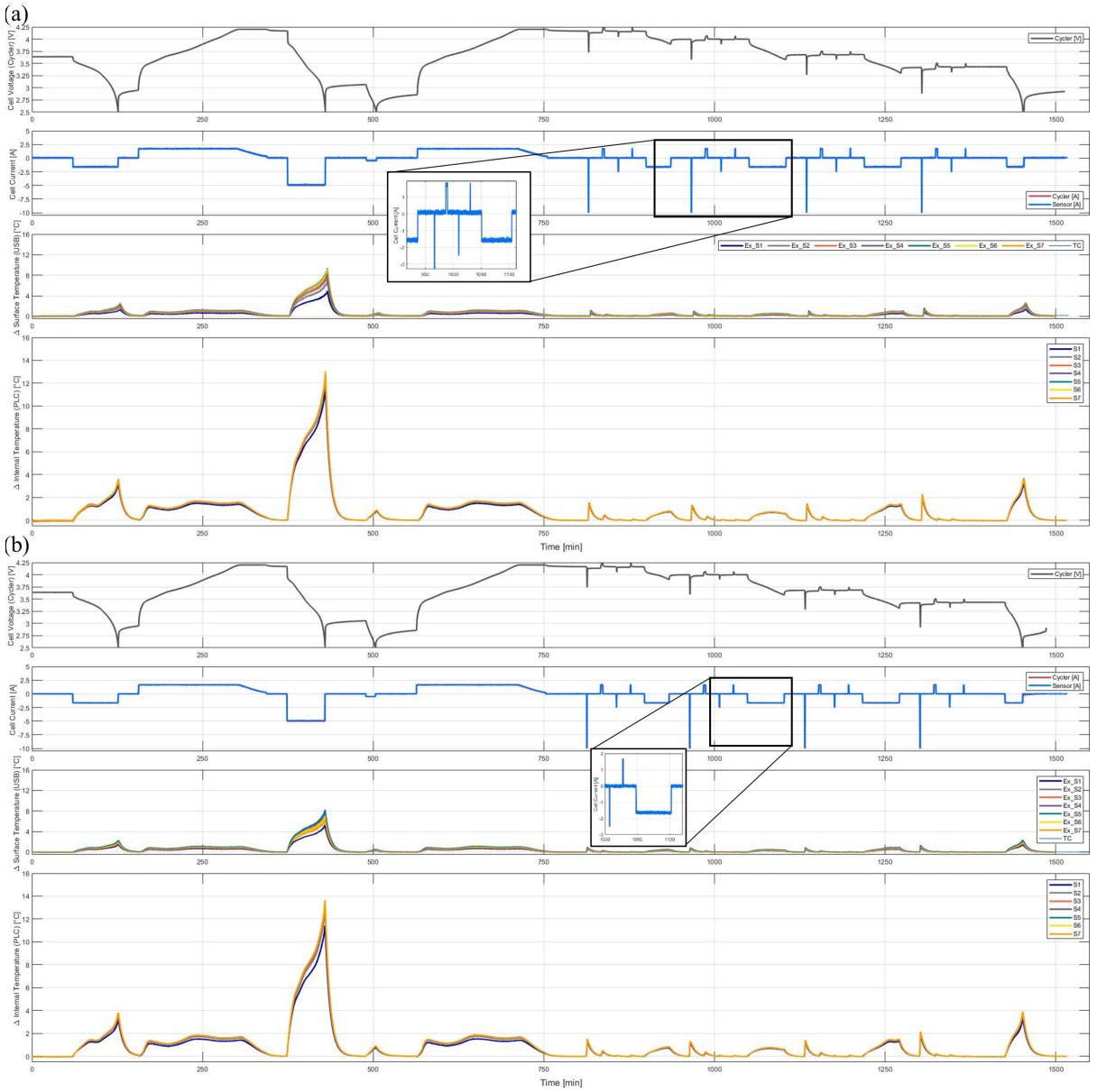

FIGURE 8. RPT performed post-cycling, plots showing voltage (cycler data), current (cycler and cell sensor data), surface temperature and internal temperature (cell sensor data), for (a) cell 3 and (b) cell 4. Notation 'S' refers to sensor, 'Ex' to external/surface measurement.

in Figs. 8 (a) and (b), respectively. The inset current plots demonstrate the current sensors have the ability to measure peaks in current charge/discharge and provide comparable data to the reference cycler measurement.

The rapid degradation of a cell during the early stages of its life is consistent with data published in the literature [55]–[57]. It has been reported that aging can be categorized into three stages: Solid Electrolyte Interphase (SEI)

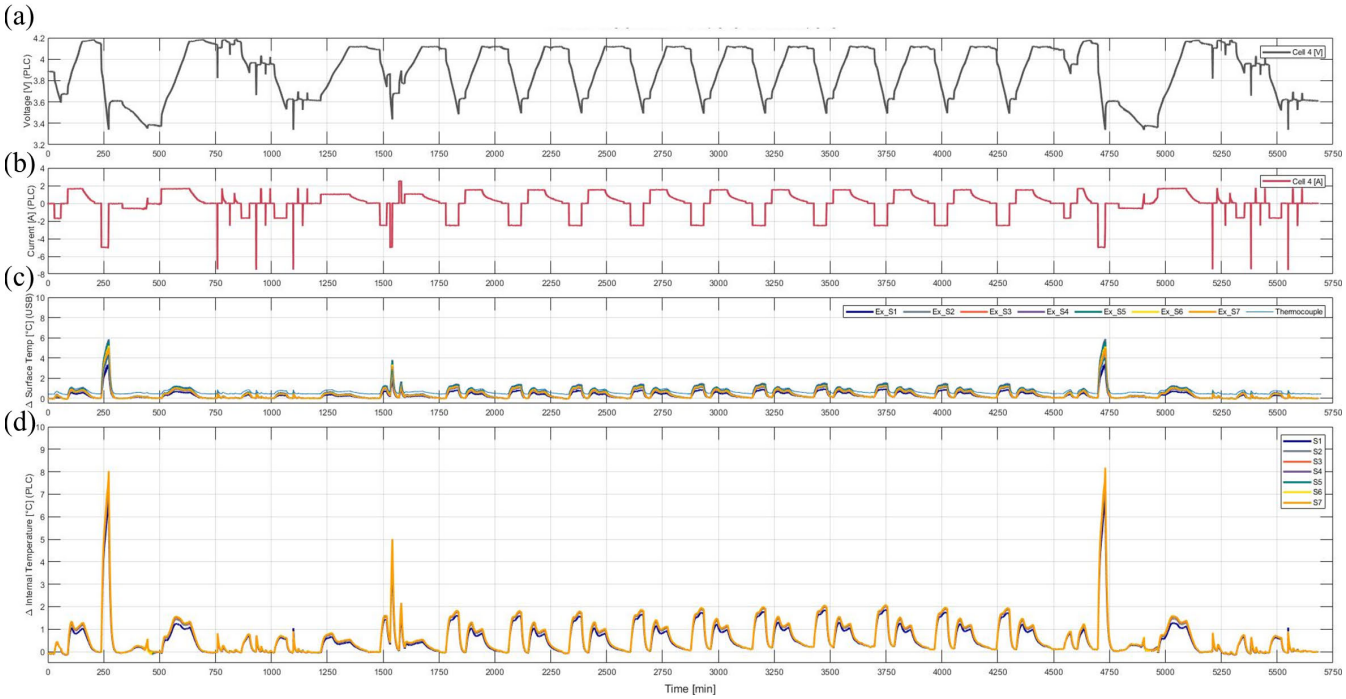

FIGURE 9. Cell Cycling experiment sensor data Cell 4, (a) voltage (logged via PLC), (b) current (PLC), (c) external temperature (USB) and (d) internal temperature (PLC).

formation (initial rapid), continuous growth of SEI, continuous loss of electrolyte (longest, middle stage of aging, during most of cell's life) and finally, past the knee point – where lithium plating, loss of active material occurs [58]. During this early stage of the cells life (the first 100 cycles, compared to long cycling experiments in the order of multiple 100s of cycles [56]) the cell performance is likely to degrade at a faster rate. In future work, instrumented cells will be compared to pristine cells over a longer period of cycles and potentially cell storage, to analyze if, or by how much, our instrumentation effects performance.

B. PLC VERIFICATION (CAN DATA COMPARISON)

To confirm the reliability and consistency of the PLC data, this experiment was constructed to transmit data at the maximum desired sampling rate (10 Hz) from all 4 cells for comparison against an automotive standard CAN bus. The controller was configured to operate in CAN-FD mode, thus enabling longer message lengths, so identical resolution of data could be sent via CAN, USB and PLC - however, as well as identical message lengths, completely identical sensor data was desired, thus the interface board must handle all data processing.

It is noted this entails extra load on the microcontroller, where a not-insignificant period of microcontroller processing time (found to be at least 5ms) is required to prepare and send the data to the CAN interface hardware. This compounds delay into the microcontroller program (i.e. each transmission method requiring in the order of a few milliseconds to prepare and send data), which would normally be avoided if only transmitting via PLC. Thus, performance here is considered worst-case.

A typical data plot acquired from the PLC sensor output for a cell is shown in Fig. 9, where (a) voltage, (b) current and (d) internal temperature are logged for cell 4 (10 Hz continuous). Plot (c) demonstrates external surface temperature measurements (logged via USB), along with a reference thermocouple (attached to the center, external of cell). Temperature data is displayed relative to the ambient environmental temperature (25 °C). Minimal increase in temperature is experienced during the 10 C/2 discharge and C/3 charge cycles (2 °C peak after charge, above ambient) from each cycle. The maximum increase in temperature (S7, nearest positive terminal records 8.0 °C above ambient), during the 30 min 1C discharge events, occurring at circa 250 min and 4750 min into the experiment time.

Hottest regions near the positive tab have previously been reported [59], where the high thermal resistivity of the positive tab and electrode architecture has been noted to cause increased heat generation [41].

Comparable internal temperature data is shown for Cells 1, 2 and 3 in Fig. 10, (a), (b) and (c), respectively. The inset plots demonstrate the need for internal temperature sensing. Compared to external temperature data, the internal sensors record around 2.3 °C lower on average, at the end of the first 1C discharge step (circa 300 min time in experiment). Typically, greater fluctuations in internal temperature are observed, highlighting the need to understand internal

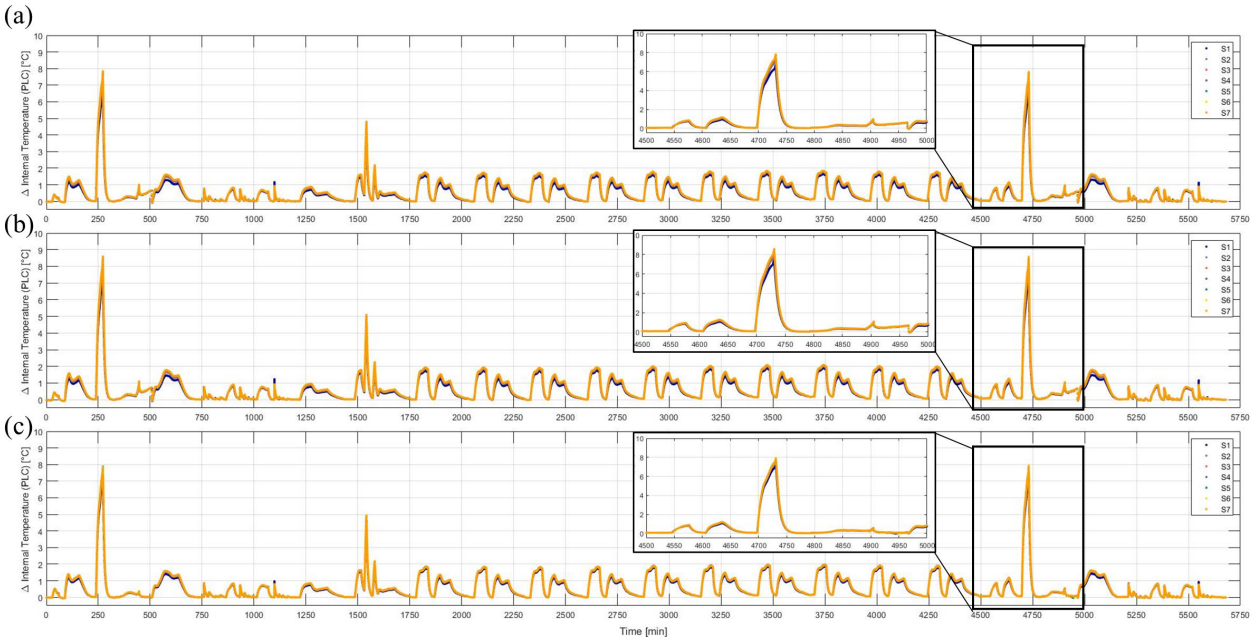

FIGURE 10. Internal temperature data for cells 1, 2 & 3, (a), (b) and (c), respectively, logged via PLC.

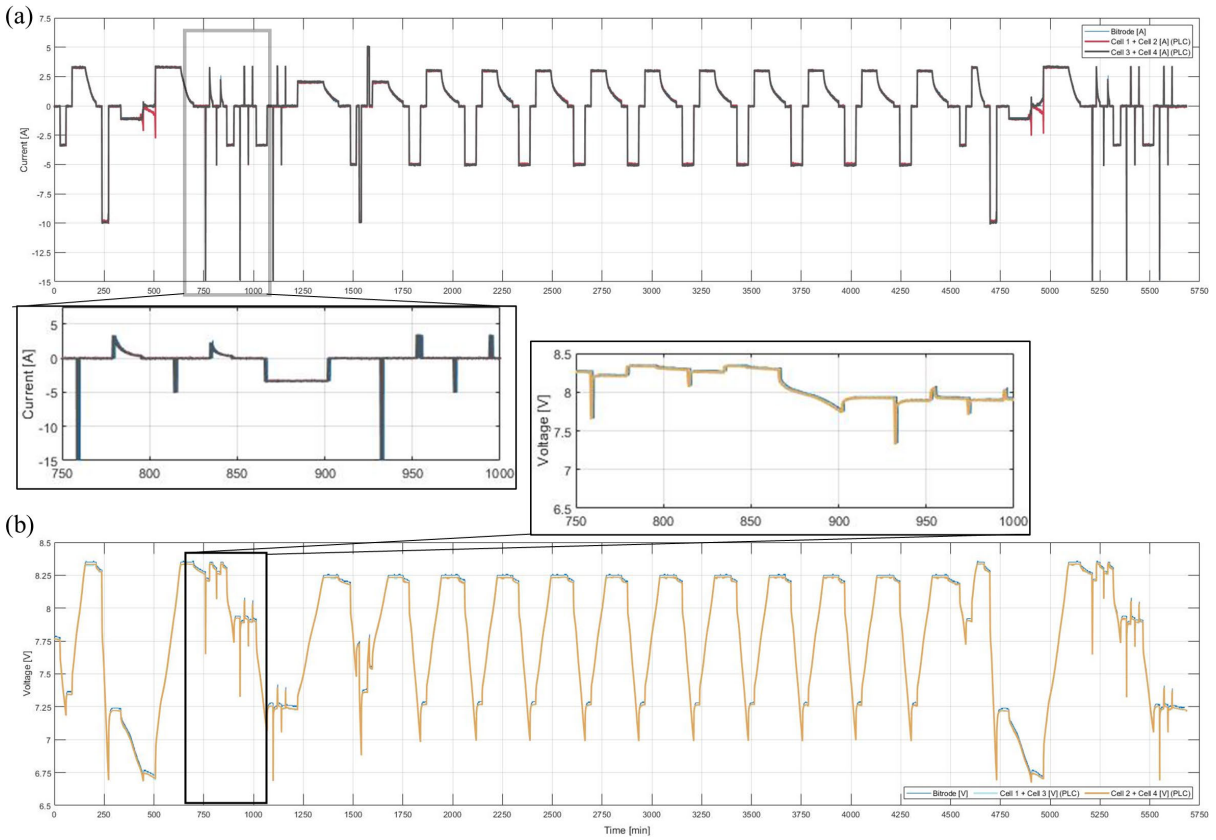

FIGURE 11. Current (a) and voltage (b) data logged via PLC, compared to reference data from module cycler for all 4 cells (summed in parallel for voltage, in series for current).

operation of the cells, with regard to predicting cell lifetime (and potentially end of life or the possible onset of thermal runaway events [3]).

For these four cells tested, the temperature gradient in general trends hottest at positive terminal (S7) and coolest at negative terminal (S1), typically 1.2 °C peak variation

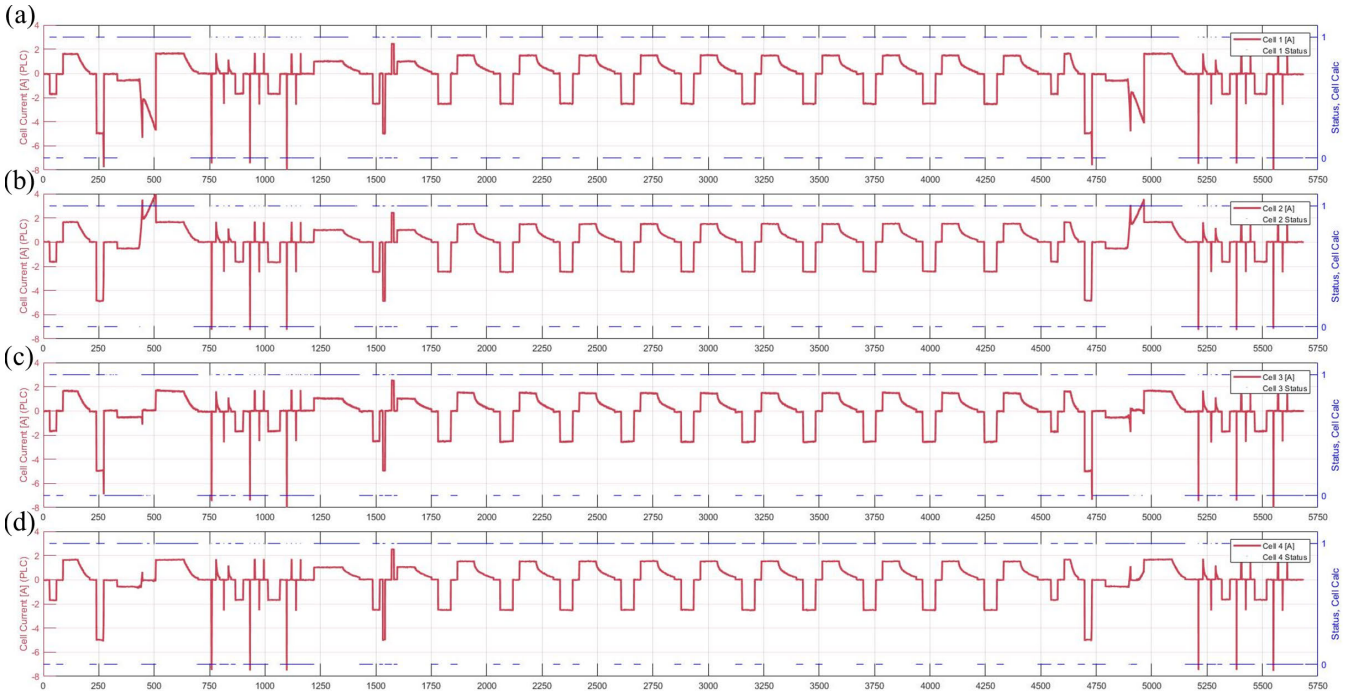

FIGURE 12. Status value calculated via cell microcontroller and transmitted to master via PLC, (a) cell 1, (b) cell 2, (c) cell 3 and (d) cell 4. Status value is predominately determined in this experiment via current measurements. All data logged at 10 Hz; status 0 indicates low current demand (<0.5 A), while status 1 indicates higher demand.

noted, for example at second 1C discharge at approximately 4700 min experiment time.

To verify the operation of the current and voltage sensors, data were summed for the current and voltage for comparison against the module cycler reference. For the 2S2P configuration, current was summed for each of the two pairs (Cell 1 and Cell 2; Cell 3 and Cell 4), shown in Fig. 11 (a). Voltage was summed for each of the series strings (Cell 1 and Cell 3; Cell 2 and Cell 4), Fig. 11 (b), for comparison against the total module values recorded by the cycler. The inset plots demonstrate the sensors show excellent correspondence to the cycler values, in terms of quantity measured and response time.

During the experiment, the status from each cell was recorded and categorized according to the three states defined in Table 3, i.e. either low demand operation (nominal, <0.5 A current demand, status value 0), standard operation (>0.5 A current, status value 1) or high demand (>40 °C, not reached during this experiment, status value 2). In this experiment, the status was not used to determine data transmission frequency; it was only used to verify state identification and reporting.

Fig. 12 shows the cell status values for cells 1, 2, 3 and 4, in plots (a), (b), (c) and (d), respectively, on the right-hand y axis. The current measurements, plotted on the left-hand y axis, were the predominate information used on an individual cell interface board level, to determine the necessary logging status reported to the master controller. The status calculation was successfully reported for all the cells, where during rest conditions in the cycle, low demand was correctly reported.

To verify the reliability of the PLC system, in terms of message loss or bit errors, a comparison was performed between the data received by the CAN and PLC systems. Fig. 13 plots (a) to (d) show cells 1 to 4 data respectively. Here, temperature data for sensors S1, S3, S5 and S7 is shown for each cell (both CAN and PLC transmitted data shown) – dashed lines indicate PLC data, dotted lines indicate CAN data. The inset plots show the success of the PLC setup, where the dashed and dotted lines overlap. Error points are indicated with crosses; in the majority of cases it was found two sets of cell data had collided in the PLC channel, thus half of the first cell's data was missing. In all these cases, this line was all marked as an error. Due to the large dataset (>3.4 million lines in total), the partial data could be recovered for each line, thus it was marked entirely as an error.

Overall, during the nearly 100 hour experiment, logged at 10 Hz, for cells 1, 2, 3 and 4, a total of 89, 22, 29 and 28 errors were identified per cell, respectively. The greatest error rate was observed for cell 1 (0.025 %), and lowest for cell 2 (0.003%). It is likely these are worst case error rates, considering the extra processing load discussed above, due to handling and transmitting data on the single microcontroller (per cell) on the three different channels. In preliminary experiments, without requiring CAN transmission, 0 bit or line errors were identified, albeit in shorter experiments (less than 50 hours). CAN bit error rates in the order of 3.1 × 10-9 have been reported ([60], although these were reported in a 'normal' environment. It is noted this is a best-case error rate, and it is not related to cell cycling or a possible future

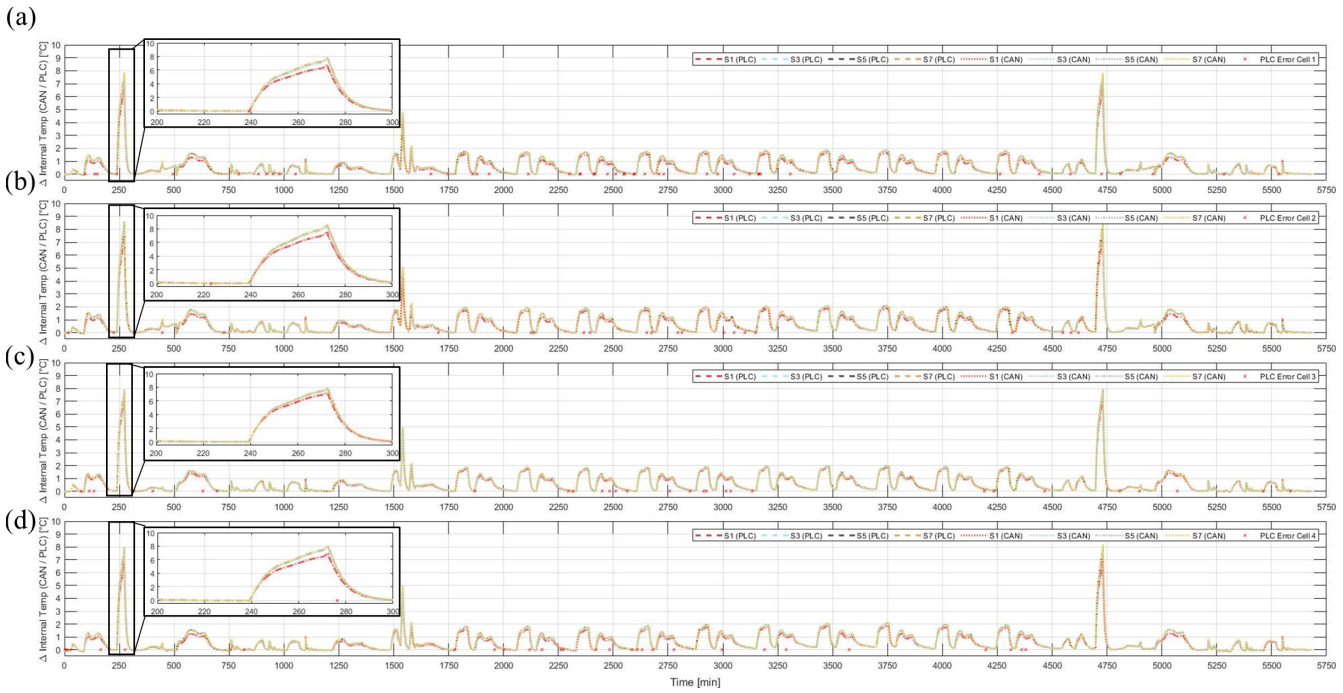

FIGURE 13. Error comparison CAN reference compared to PLC data, cells 1, 2, 3 and 4 shown in plots (a), (b), (c) and (d), respectively.

BMS application. In our experiment, in the locations where errors are detected, they are in-general widely distributed across the duration of the experiment. For Cells 2, 3 and 4 two error never occur within a 1 min period. The data processing algorithms appear to impact the first cell sampled in the program greater (i.e. cell 1), which as well as having the higher error rate, around a quarter of the errors repeat within the same 1 min period, noted by the overlapping error markers on Fig. 13 (a). The success of these experiments verified the ability of our PLC system to provide comparable results to a known communication standard, satisfying objective (i).

C. DRIVE CYCLE ADAPTIVE SAMPLING

We have previously demonstrated an iteration of our PLC network with the drive cycle profile (results shown in [14] for comparison), and here we perform the same current profile on our 2S2P cell arrangement, with PLC data acquisition. However, in this case, the data transmitted via the power line is sampled at an adaptive rate, depending predominately on the current demand from the cell (temperature deviation around ambient is minimal for this profile with 2S2P cell layout).

The output data recorded for cell 4 is shown in Fig. 14, with (a) voltage, (b) current and (d) internal temperature recorded via PLC (adaptive sampling). The surface temperature (c) was recorded via a dedicated wired USB connection. In the PLC adaptive plots, all data points are identified with markers (no lines, as points may not be contiguous). On plots (a) and (b), the lighter colored points indicate 0.2 Hz sampling rate and darker colored points indicate 5 Hz sampling rate; in (d) only single colors were used (this is for simplicity, as during 5 Hz sampling condition, all 7 sensors are shown together). The current sensor data is constantly logged at 16 bit resolution (this is due to only experiencing minimal current changes, relative to the full scale range of the sensor). Voltage data is logged at both 8 bit (low sampling rate) and 16 bit resolutions. Periods of lower current draw during the cycle (i.e. circa between 20 min and 38 min) demonstrate lower demand from the cell causing the status to fall to nominal (and thereby reducing the sampling rate to 0.2 Hz, with corresponding minimal sensor data transmitted via PLC).

Plot (d) indicates the adaptive sampling rate where the abrupt steps in delta temperature (relative to ambient, 25 °C) are due to the lower resolution (8 bit when sampling 0.2 Hz, opposed to 16 bit when faster sampling employed). This causes a minor digitization error, indicated by the step changes in temperature (noticeable in the results, when switching from a period of intense data logging with all 7 sensors to short periods of logging only 2 sensors at lower resolution. During the experiment sampling at the highest rate (i.e. experiment time from around 25 to 57 min), the temperature gradient observed above (S7 hottest, S1 coolest) is maintained. In this period, data from all 7 thermistors is recorded. Post drive cycle (30 min period of rest allowed at the end of experiment), the coolest sensor recorded switched to S5, although previous data during rest periods, e.g. Fig. 10, indicates there is minimal difference between sensor readings (less than 0.5 °C). 8-bit resolution temperature readings correspond to approximately 0.5 °C step in temperature change (thermistors produce logarithmic response to temperature, thus this step size varies).

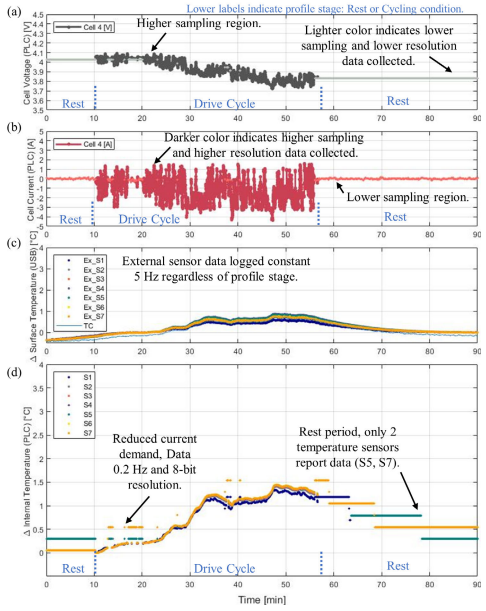

FIGURE 14. Drive cycle (a) voltage, (b) current, (c) external temperature and (d) internal temperature for cell 4. Plots (a), (b) and (d) logged via adaptive sampling rate PLC.

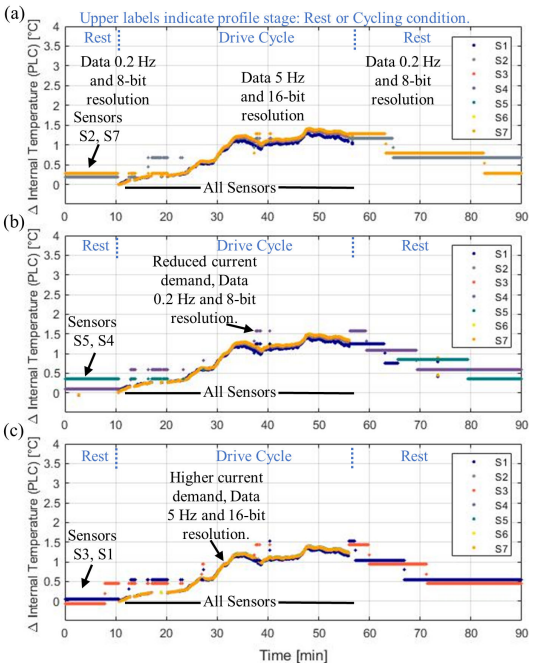

FIGURE 15. Drive cycle internal cell temperature logged at 0.2 Hz (rest periods, notably initial 10 min, final 30 min) and 5 Hz (during the period between 10 to 60 min) data rate, for cells 1, 2 and 3 in plots (a), (b) and (c), respectively.

These step changes are visible in the internal temperature Fig. 15 plots (a), (b) and (c) for cells 1, 2 and 3, respectively, where during cooling (in the period beyond 60 min in experiment time) there are large (0.5 °C) steps visible.

The regular switching between coolest sensor, cell 2 (b) at around 65 min, is due to the minimal difference between sensors S5 and S1.

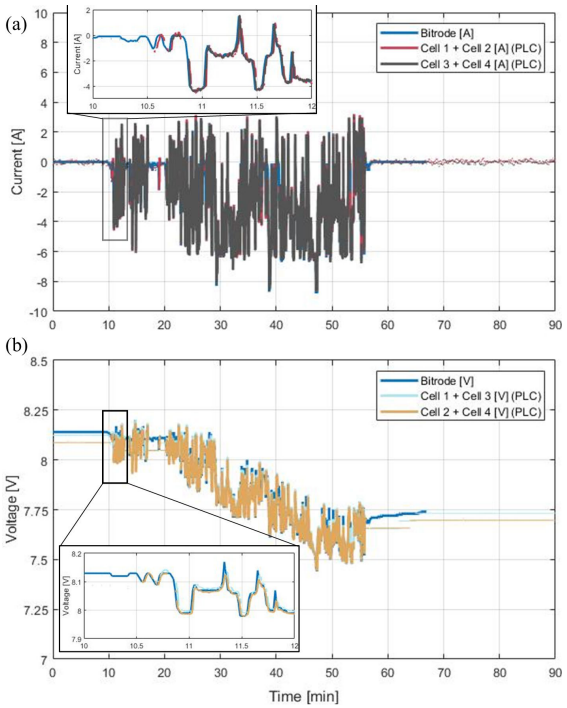

FIGURE 16. Current (a) and voltage (b) summed for cells 1 to 4, in 2S2P arrangement during adaptive sampling drive cycle profile.

The initial phase of the drive cycle causes the current demand from each cell to be greater than 0.5 A, triggering the 5 Hz logging period. Fig. 16 (a), inset enlarged view of this period, shows the increase in sampling rate. This sampling rate shows excellent correspondence to the cycler data, during the transient current variation. Data is summed in Fig. 16 for current and voltage, as detailed in Fig. 11. The initial summed data for cells 2 and 4, Fig. 16 (b), demonstrate a lower voltage is initially reported for this cell pair. However, this error is due to lower sampling resolution (8 bit), causing a visible offset (nearly 0.05 V) compared to the cycler data (similarly, cell pair 1 and 3 voltage lie around 0.02 V below cycler). The inset plot demonstrates this offset is alleviated at 16 bit resolution.

The adaptive sampling method of data collection reduces bandwidth requirements for the PLC system, allowing scalability to a larger number of cells, without sacrificing individual cell reporting speed when urgent messages are needed. In the microcontroller the 16 bit value is decimated to 8 bit before transmission (therefore coolest and hottest values are determined with complete 16 bit resolution). E.g., graphing post-processing, an increment from decimal 84 to 83 equals rise of temperature from 25.2 to 25.7 °C. The volume of data collected is reduced by around 65 % by implementing this strategy (complete 5 Hz dataset logged via CAN circa 11.7 mb, compared to 4.1 mb, logged via adaptive PLC). Minimal key features of the data are lost by reducing the sampling rate and sensor reported resolution during the low activity periods. The high performance of our sensor system, notably current sensor, in this experiment (ability to detect currents less than 1 A to above 10 A) has satisfactorily

demonstrated objective (ii), showing the transient profile does not interfere with PLC nor show flaws in sensor performance.

D. EXTERNAL HEATING ADAPTIVE SAMPLING

The drive cycle profile demonstrated current sensor measurements can indicate periods of rest. To demonstrate temperature sensing may also be required to trigger key logging periods, an external silicon heater was used to increase the internal cell temperature from ambient (25 °C, inside a controller climatic chamber) to a maximum of 40 °C. A single cell was used, with the heater pad wrapped around the cell towards the positive end of the can.

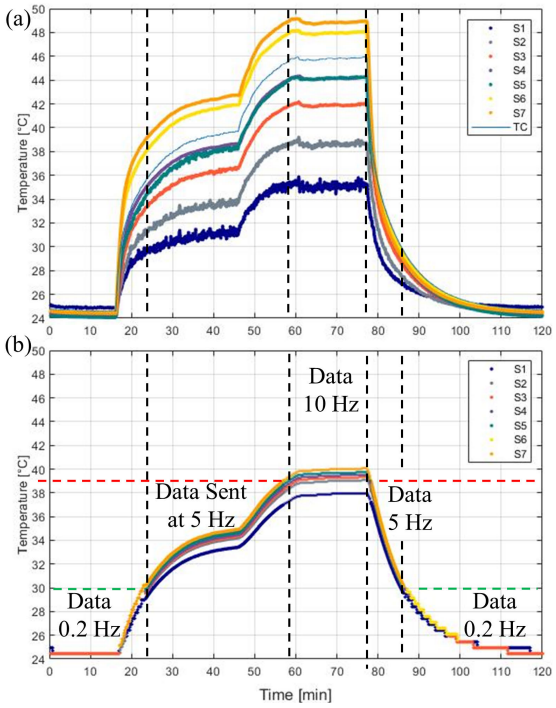

FIGURE 17. Temperature data for one cell when external heating pad applied, (a) external temperature and (b) PLC adaptive internal temperature data.

Fig. 17 demonstrates the (a) external thermistor array data plot and (b) internal thermistor plot (logging at 0.2, 5 and 10 Hz, dependent on temperature recorded). The temperature level to transmit data at 10 Hz was lowered to 39 °C (to prevent heating the external temperature measured by the reference thermocouple to above 45 °C for safety reasons).

The internal compared to external temperature plots (see vertical dashed lines in plot (a)) indicate the time delay (order of 5 to 8 min) for the temperature to propagate from the surface to core of the cell.

The reduced sampling rate (temperature less than 30 °C) and reduced sensors sampled (hottest and coolest only), Fig. 17 (b), do not lose significant information from the plot. At higher temperatures (i.e. circa 70 min) there is a larger temperature gradient (S7 hottest, around 40.5 °C, S1 coolest – furthest from the heater nearly 37.9 °C) demonstrate the need to record the temperature along the core of the cell, when a hot spot affects only a portion of the cell. The aluminum construction and jelly roll layers have a relatively low cross-plane thermal conductivity in this direction [42]. This experiment has demonstrated objective (iii) is complete, where an interrupt can be generated during firstly high current demand and secondly abnormal temperature detection. Bi-directional communication is essential for this purpose (where sampling rate and resolution of data transmitted) is dictated by the master.

In addition to external heating sources, hot spots can form as manufacturing tolerances propagate over the life of a cell [61]; these flaws can initially effect a small region of the cell [62], before eventually potentially leading to thermal runway. Early detection of these events is desired [39], thus leading our drive to thorough cell instrumentation.

V. CONCLUSION

In this work we have demonstrated the functionality of our PLC system with 4 instrumented cells, arranged in a 2S2P configuration. This system demonstrates the path towards smart cells, where sensors and communication circuitry can be embedded directly within a cell. This could lead to the direct replacement of passive cells (without circuitry or sensors) with smart cells, enabling next generation EVs and aircraft to be safely equipped with high-capacity battery packs for improved range and longer vehicle life time.

In this work we instrumented the four 21700 cells (5 Ah capacity), with arrays of thermistor sensors (10 mm spatial resolution through core of cell). Additionally, the voltage of the cell was logged (analogue data logged at 16 bit resolution, via dedicated ADC) and current data (Hall Effect sensor, uniquely mounted on cell bus bar).

We determined the sensor instrumentation process had minimal effect on the performance of our cells during our testing. Measurements of the cell impedance (1 kHz) demonstrated minimal variance during the instrumentation process (average increase, around 0.4 mΩ, verified from pristine, post-drilling to post-instrumentation). Cell capacity, measured via our RPT, also demonstrated minimal variation, beyond that expected from equipment and connection tolerances (loss of 0.03 Ah, approximately 0.63 %).

We defined three objectives to verify the operation of our PLC system. Firstly, to verify operation against a known standard (CAN). We chose a data rate of 10 Hz for our 4 cells (perhaps limited by the low bandwidth UART, 115.2 kbps link from the microcontroller to PLC modem) to be transmitted over the power-line. We verified our system was able to successfully transmit almost 3.4 million messages, with a low error rate (0.005 % overall), throughout an experiment involving cycling cells up to 2C discharge rate. It was noted the extra burden on the system, where to allow identical data to be transmitted, a single microcontroller per cell was used to initiate transfers via PLC, USB and CAN for each message. The PLC network required substantially lower power consumption (150 mW, including LED indicators, compared to CAN 220 mW) during experimentation.

Secondly, we tested the communication network with a transient drive cycle profile, with adaptive data logging. This verified the system could log data at a reduced sampling rate (0.2 Hz) and resolution (reduced to 8 bit from full ADC 16 bit) during periods of inactivity (less than 0.5 A current demand, temperature ±5 °C ambient). The sensors demonstrated excellent performance, with the current sensor able to accurately record the drive cycle profile. No abnormal responses (transient spikes or erroneous data) were logged during the experiment. A reduction of recorded data file size of 65 % was achieved over the 90 min experiment (comparing logging constant 5 Hz to adaptive).

Finally we tested the ability of each individual cell being able to generate an interrupt, to sample faster when a key feature (increase current or temperature) was detected. This aims to show the scalability of the system, where multiple cells can be sampled at different rates. The drive cycle profile demonstrated sampling at 0.2 Hz (rest) or 5 Hz (active current profile); an external heater was employed to demonstrate abnormal temperatures (above 40 °C) cause the maximum defined data transmission rate (10 Hz) to be requested. The heating profile (capturing regions from ambient, 25 °C, through active between 30 to 40 °C and high, above 40 °C) demonstrated the three desired sampling rates were correctly assigned.

These tests further our goal to create a smart cell with internally embedded circuitry. The reliable operation of these cells over 100s of hours of testing has demonstrated their potential for the applications of cell modelling and battery cooling system development. Additionally, we believe smart cells will be required for the electrician of the aerospace and heavy transportation industries.

VI. FURTHER WORK

A. PLC DEVELOPMENT

In this work, as a first study of PLC with an instrumented cell, we reduced the voltage operation range of the module to greater than 3.3 V per cell, enabling each cell to maintain sufficient voltage to operate a LDO regulator. Preliminary studies using a buck-boost regulator have demonstrated PLC performance remains excellent across full SoC (2.5 to 4.2 V), however the lower efficiency of the regulator causes increased power demand (+50 %). Future work will aim to overcome this limitation; proposals include reducing power consumption (i.e. removal of indicator LEDs, etc.); or combined buck-boost and LDO at lower voltage (microcontroller can operate at 2.5 V, thus only enable 3.3 V buck-boost regulator when operation of 3.3 V components is required).

A single 5 MHz transmission frequency was selected in this work for the PLC. The modem enables selectable frequencies, thus potentially enabling frequency division multiplexing, to be tested. The current communication bandwidth was reduced to the baud rate accessible on the microcontroller UART interface pins (115.2 kbps). The maximum recommended rate for this TI PLC modem is 500 kbps, using the RS-485 protocol. Higher baud rates should be trialed to optimize the bandwidth of the PLC system and enable scalability to larger modules. Furthermore, improvement of redundancy checks on PLC messages could further decrease error rates.

This study has demonstrated the low bit errors achieved with a single frequency, and OOK protocol. We aim to investigate the impedance spectrum of these cells and module configuration to optimize the transmission frequency and encoding protocol. This could be supported via modelling work, to understand the operation of our PLC network.

In future work we aim to trial the system with a larger module size, to help understand the performance (bit error rates, transmission speed and reliability) when operating with a larger number of cells. This will also lead to assessing cell to cell communication, and avoiding the need for a single master (point of failure) in the system. This will help demonstrate the improved safety, robustness and redundancy of our distributed BMS.

B. CELL INSTRUMENTATION

These prototype smart cells incorporated sensors for temperature, voltage and current. Further parameters are of interest to cell modelling, such as pressure or gas composition. Via our M2.5 thread inlet into the cell, further sensor types can be connected or other components inserted (such as a reference electrode). These sensors must be tested inside the cylindrical cells for a greater number of cycles (at least 100 cycles) to demonstrate their long-term reliability, and ability to monitor cell performance during its lifetime and aging processes. Independently, the longevity of the sensor components will be quantified. For example, the sensors with flexible coating, can be emerged in a chemical bath of electrolyte (potentially heated above ambient), for a period of several weeks to demonstrate their resilience to the harsh environment.

To fully utilize instrumented cells with self-powered sensors, a memory chip should be installed within the interface circuitry, thus enabling self-logging of events over the life time of the cell. This would aid pack servicing and help select cells for second life applications. To interface with these additional ICs, and perhaps a wider range of digital sensors, further break-out capabilities, such as I2C will be considered for future PCB revisions.

In this work the RPT was not performed with the PLC system in operation, due to concerns of influencing capacity readings. In future work, following the reference data collected here, these RPTs could be repeated with logging via PLC. The RPT or cycler operation would need adapting (to avoid triggering the safety cut-off of the cycler, if the voltage were to drop below 2.5 V, due to the cell also powering the sensors at 0 % SoC).

REFERENCES

[1] T. Grandjean, A. Barai, E. Hosseinzadeh, Y. Guo, A. McGordon, and J. Marco, "Large format lithium ion pouch cell full thermal characterisation for improved electric vehicle thermal management," *J. Power Sources*, vol. 359, pp. 215–225, Aug. 2017, doi: 10.1016/j.jpowsour.2017.05.016.

[2] X. Lin, H. E. Perez, J. B. Siegel, and A. G. Stefanopoulou, "Robust estimation of battery system temperature distribution under sparse sensing and uncertainty," *IEEE Trans. Control Syst. Technol.*, vol. 28, no. 3, pp. 753–765, May 2020, doi: 10.1109/TCST.2019.2892019.

[3] R. R. Richardson, S. Zhao, and D. A. Howey, "On-board monitoring of 2-D spatially-resolved temperatures in cylindrical lithium-ion batteries: Part II. State estimation via impedance-based temperature sensing," *J. Power Sources*, vol. 327, pp. 726–735, Sep. 2016, doi: 10.1016/j.jpowsour.2016.06.104.

[4] N. Tarle, R. Kulkarni, N. Desale, and V. Pawar, "Design of a battery management system for formula Student electric race vehicle," in *Proc. 5th Int. Conf. Comput., Commun., Control Autom. (ICCUBEA)*, Sep. 2019, pp. 1–6, doi: 10.1109/ICCUBEA47591.2019.9128526.

[5] D. Xu, L. Wang, and J. Yang, "Research on li-ion battery management system," in *Proc. Int. Conf. Electr. Control Eng.*, Jun. 2010, pp. 4106–4109, doi: 10.1109/iCECE.2010.998.

[6] H. A. Gabbar, A. M. Othman, and M. R. Abdussami, "Review of battery management systems (BMS) development and industrial standards," *Technologies*, vol. 9, no. 2, p. 28, Apr. 2021, doi: 10.3390/TECHNOLOGIES9020028.

[7] A. Reindl, H. Meier, and M. Niemetz, "Scalable, decentralized battery management system based on self-organizing nodes," in *Proc. Int. Conf. Archit. Comput. Syst.* (Lecture Notes in Computer Science), vol. 12155. Cham, Switzerland: Springer, 2020, pp. 171–184, doi: 10.1007/978-3-030-52794-5_13.

[8] T. Cai, P. Valecha, V. Tran, B. Engle, A. Stefanopoulou, and J. Siegel, "Detection of li-ion battery failure and venting with carbon dioxide sensors," *eTransportation*, vol. 7, Feb. 2021, Art. no. 100100, doi: 10.1016/j.etran.2020.100100.

[9] T. Faika, T. Kim, and M. Khan, "An Internet of Things (IoT)-based network for dispersed and decentralized wireless battery management systems," in *Proc. IEEE Transp. Electrific. Conf. Expo (ITEC)*, Jun. 2018, pp. 342–346, doi: 10.1109/ITEC.2018.8450161.

[10] S. Jeschke, J. Loos, and M. Kleinen, "Impact of highly efficient power electronics on the EMC in electric vehicles with autonomous driving functions," in *Proc. Automot. Meets Electron.; 11th GMM-Symp.*, Mar. 2020, pp. 1–4.

[11] A. Misra, "Energy storage for electrified aircraft: The need for better batteries, fuel cells, and supercapacitors," *IEEE Electrific. Mag.*, vol. 6, no. 3, pp. 54–61, Sep. 2018, doi: 10.1109/MELE.2018.2849922.

[12] A. Bauen, N. Bitossi, L. German, A. Harris, and K. Leow, "Sustainable aviation fuels: Status, challenges and prospects of drop-in liquid fuels, hydrogen and electrification in aviation," *Johnson Matthey Technol. Rev.*, vol. 64, no. 3, pp. 263–278, Jul. 2020, doi: 10.1595/205651320x15816756012040.

[13] G. M. Cavalheiro, T. Iriyama, G. J. Nelson, S. Huang, and G. Zhang, "Effects of nonuniform temperature distribution on degradation of lithium-ion batteries," *J. Electrochem. Energy Convers. Storage*, vol. 17, no. 2, May 2020, Art. no. 021101, doi: 10.1115/1.4045205.

[14] T. A. Vincent and J. Marco, "Development of smart battery cell monitoring system and characterization on a small-module through in-vehicle power line communication," *IEEE Access*, vol. 8, pp. 220658–220671, 2020, doi: 10.1109/ACCESS.2020.3043657.

[15] T. A. Vincent and J. Marco, "Development of smart battery cells through sensor instrumentation and in-vehicle power line communication," in *Proc. IEEE Int. Symp. Power Line Commun. Appl. (ISPLC)*, May 2020, pp. 1–5, doi: 10.1109/ISPLC48789.2020.9115411.

[16] C. Cano, A. Pittolo, D. Malone, L. Lampe, A. M. Tonello, and A. G. Dabak, "State of the art in power line communications: From the applications to the medium," *IEEE J. Sel. Areas Commun.*, vol. 34, no. 7, pp. 1935–1952, Jul. 2016, doi: 10.1109/JSAC.2016.2566018.

[17] Z. Sheng, D. Tian, V. C. M. Leung, and G. Bansal, "Delay analysis and time-critical protocol design for in-vehicle power line communication systems," *IEEE Trans. Veh. Technol.*, vol. 67, no. 1, pp. 3–16, Jan. 2018, doi: 10.1109/TVT.2017.2770182.

[18] A. Pittolo, M. De Piante, F. Versolatto, and A. M. Tonello, "In-vehicle power line communication: Differences and similarities among the in-car and the in-ship scenarios," *IEEE Veh. Technol. Mag.*, vol. 11, no. 2, pp. 43–51, Jun. 2016, doi: 10.1109/MVT.2015.2480098.

[19] M. Brandl, K. Kellner, T. Posnicek, and D. Hochwarter, "Performance evaluation of a DQPSK and a DSSS PLC-modem for vehicular applications," in *Proc. IEEE Int. Symp. Power Line Commun. Appl. (ISPLC)*, Apr. 2019, pp. 1–5, doi: 10.1109/ISPLC.2019.8693264.

[20] M. Antoniali, M. Girotto, and A. M. Tonello, "In-car power line communications: Advanced transmission techniques," *Int. J. Automot. Technol.*, vol. 14, no. 4, pp. 625–632, Aug. 2013, doi: 10.1007/s12239-013-0067-2.

[21] Y.-H. Zhang, S.-X. Lin, L.-B. Chen, W.-J. Chang, W.-W. Hu, J.-J. Tang, and C.-T. Yu, "An implementation of an in-vehicle power line communication system," in *Proc. IEEE 6th Global Conf. Consum. Electron. (GCCE)*, Oct. 2017, pp. 1–2, doi: 10.1109/GCCE.2017.8229422.

[22] T. F. Landinger, G. Schwarzberger, M. Rose, S. Dollhaeubl, G. Hofer, A. P. Talei, and A. Jossen, "Power line communications in automotive traction batteries: A proof of concept," in *Proc. IEEE Int. Symp. Power Line Commun. Appl. (ISPLC)*, May 2020, pp. 1–5, doi: 10.1109/ISPLC48789.2020.9115412.

[23] M. S. Saleem, "Development of PLC based communication architecture for battery management system," in *Proc. IEEE 91st Veh. Technol. Conf. (VTC-Spring)*, May 2020, pp. 1–5, doi: 10.1109/VTC2020-Spring48590.2020.9128451.

[24] A. P. Talie, W. A. Pribyl, and G. Hofer, "Electric vehicle battery management system using power line communication technique," in *Proc. 14th Conf. Ph.D. Res. Microelectron. Electron. (PRIME)*, Jul. 2018, pp. 225–228, doi: 10.1109/PRIME.2018.8430304.

[25] J. Jousse, N. Ginot, C. Batard, and E. Lemaire, "Power line communication management of battery energy storage in a small-scale autonomous photovoltaic system," *IEEE Trans. Smart Grid*, vol. 8, no. 5, pp. 2129–2137, Sep. 2017, doi: 10.1109/TSG.2016.2517129.

[26] W.-W. Hu, F.-L. Chang, Y.-H. Zhang, L.-B. Chen, C.-T. Yu, and W.-J. Chang, "Design and implementation of a next-generation hybrid internet of vehicles communication system for driving safety," *J. Commun.*, vol. 13, no. 12, pp. 737–742, 2018, doi: 10.12720/jcm.13.12.737-742.

[27] C. Mikolajczak, M. Kahn, K. White, and R. T. Long, "Introduction to lithium-ion cells and batteries," in *Lithium-Ion Batteries Hazard and Use Assessment*. Boston, MA, USA: Springer, 2011, pp. 1–24.

[28] W. Choi, H. C. Shin, J. M. Kim, J. Y. Choi, and W. S. Yoon, "Modeling and applications of electrochemical impedance spectroscopy (EIS) for lithium-ion batteries," *J. Electrochem. Sci. Technol.*, vol. 11, no. 1, pp. 1–13, 01-Feb-2020.

[29] M. J. Koshkouei *et al.*, "Evaulation of an *in situ* QAM-based power line communication system for lithium-ion batteries," *IET Electr. Syst. Transp.*, pp. 1–11, 2021, doi: 10.1049/els2.12033.

[30] R. Sabir, A. Bloemeke, N. Fuengwarodsakul, and D. U. Sauer, "Radio frequency impedance analysis of lithium ion cells for power line communication," in *Proc. IEEE Power Energy Student Summit*, Oct. 2020, pp. 1–6.

[31] T. F. Landinger, G. Schwarzberger, G. Hofer, M. Rose, and A. Jossen, "Power line communications for automotive high voltage battery systems: Channel modeling and coexistence study with battery monitoring," *Energies*, vol. 14, no. 7, p. 1851, Mar. 2021, doi: 10.3390/en14071851.

[32] A. Pake Talei, W. A. Pribyl, and G. Hofer, "Considerations for a power line communication system for traction batteries betrachtungen für ein powerline-kommunikationssystem für antriebsbatterien," *e & i Elektrotechnik und Informationstechnik*, vol. 138, pp. 3–14, Jan. 2021, doi: 10.1007/s00502-020-00861-2.

[33] A. R. Ndjiongue and H. C. Ferreira, "Power line communications (PLC) technology: More than 20 years of intense research," *Trans. Emerg. Telecommun. Technol.*, vol. 30, no. 7, Jun. 2019, Art. no. e03575, doi: 10.1002/ett.3575.

[34] M. Antoniali, M. De Piante, and A. M. Tonello, "PLC noise and channel characterization in a compact electrical car," in *Proc. IEEE 17th Int. Symp. Power Line Commun. Appl.*, Mar. 2013, pp. 29–34, doi: 10.1109/ISPLC.2013.6525820.

[35] I. Ouannes, P. Nickel, J. Bernius, and K. Dostert, "Physical layer performance analysis of power line communication (PLC) applied for cell-wise monitoring of automotive lithium-ion batteries," in *Proc. 18th Int. OFDM Workshop (InOWo)*, Aug. 2014, pp. 136–143.

[36] Y. Barsukov and J. Qian, *Battery Power Management for Portable Devices*. Boston, MA, USA: Artech House, 2013.

[37] *Road Vehicles—Local Interconnect Network (LIN)—Part 8: Electrical Physical Layer (EPL) Specification: LIN Over DC Powerline (DC-LIN)*, International Standards, Standard ISO/TC 22/SC 31 Data communication, Standard ISO 17987-8, 2019. [Online]. Available: https://www.iso.org/standard/71044.html

[38] T. Muneer, R. Milligan, I. Smith, A. Doyle, M. Pozuelo, and M. Knez, "Energetic, environmental and economic performance of electric vehicles: Experimental evaluation," *Transp. Res. D, Transp. Environ.*, vol. 35, pp. 40–61, Mar. 2015, doi: 10.1016/j.trd.2014.11.015.

[39] A. Fortier, M. Tsao, N. D. Williard, Y. Xing, and M. G. Pecht, "Preliminary study on integration of fiber optic Bragg grating sensors in li-ion batteries and *in situ* strain and temperature monitoring of battery cells," *Energies*, vol. 10, no. 7, p. 838, 2017, doi: 10.3390/en10070838.
[40] G. Pandian, M. Pecht, E. Zio, and M. Hodkiewicz, "Data-driven reliability analysis of Boeing 787 Dreamliner," *Chin. J. Aeronaut.*, vol. 33, no. 7, pp. 1969–1979, 2020, doi: 10.1016/j.cja.2020.02.003.
[41] Y. Yu, E. Vergori, D. Worwood, Y. Tripathy, Y. Guo, A. Somá, D. Greenwood, and J. Marco, "Distributed thermal monitoring of lithium ion batteries with optical fibre sensors," *J. Energy Storage*, vol. 39, Jul. 2021, Art. no. 102560, doi: 10.1016/j.est.2021.102560.
[42] G. Zhang, L. Cao, S. Ge, C.-Y. Wang, C. E. Shaffer, and C. D. Rahn, "*In situ* measurement of radial temperature distributions in cylindrical li-ion cells," *J. Electrochem. Soc.*, vol. 161, no. 10, pp. A1499–A1507, Jul. 2014, doi: 10.1149/2.0051410jes.
[43] J. Goldak, M. Martinez, and S. Tchernov, "Correlating large sets of experimental data with high resolution computational weld mechanics models," in *Mathematical Modelling of Weld Phenomena 12*, C. Sommitsch, N. Enzinger, and P. Mayr, Eds. Graz, Austria: Verlag der Technischen Universität Graz, 2019, p. 819.
[44] E. Bassi, F. Benzi, L. Almeida, and T. Nolte, "Powerline communication in electric vehicles," in *Proc. IEEE Int. Electric Mach. Drives Conf.*, May 2009, pp. 1749–1753, doi: 10.1109/IEMDC.2009.5075439.
[45] S. Bacquet and M. Maman, "Radio frequency communications for smart cells in battery pack for electric vehicle," in *Proc. IEEE Int. Electr. Vehicle Conf. (IEVC)*, Dec. 2014, pp. 1–4, doi: 10.1109/IEVC.2014.7056120.
[46] Texas Instruments. (2021). *Online Datasheets*. [Online]. Available: https://www.ti.com/product/THVD8000
[47] K. Matheus and T. Königseder, *Automotive Ethernet*, 3rd ed. Cambridge, U.K.: Cambridge Univ. Press, 2021.
[48] J. M. Hughes, *Arduino: A Technical Reference: A Handbook for Technicians, Engineers, and Makers*. Boston, MA, USA: O'Reilly Media, 2016.
[49] R. Gogoana, M. B. Pinson, M. Z. Bazant, and S. E. Sarma, "Internal resistance matching for parallel-connected lithium-ion cells and impacts on battery pack cycle life," *J. Power Sources*, vol. 252, pp. 8–13, Apr. 2014, doi: 10.1016/j.jpowsour.2013.11.101.
[50] D. Worwood, R. Algoo, R. J. McGlen, J. Marco, and D. Greenwood, "A study into different cell-level cooling strategies for cylindrical lithium-ion cells in automotive applications," *Int. J. Powertrains*, vol. 7, nos. 1–3, pp. 199–226, 2018, doi: 10.1504/IJPT.2018.090381.
[51] J. Fleming, T. Amietszajew, J. Charmet, A. J. Roberts, D. Greenwood, and R. Bhagat, "The design and impact of *in-situ* and operando thermal sensing for smart energy storage," *J. Energy Storage*, vol. 22, pp. 36–43, Apr. 2019, doi: 10.1016/j.est.2019.01.026.
[52] L. Somerville, S. Ferrari, M. Lain, A. McGordon, P. Jennings, and R. Bhagat, "An *in-situ* reference electrode insertion method for commercial 18650-type cells," *Batteries*, vol. 4, no. 2, p. 18, Apr. 2018, doi: 10.3390/batteries4020018.
[53] T. Amietszajew, J. Fleming, and A. J. Roberts, "Hybrid thermo-electrochemical *in situ* instrumentation for lithium-ion energy storage," *Batteries Supercaps*, vol. 2, no. 11, pp. 934–940, 2019, doi: 10.1002/batt.201900109.
[54] M. F. Niri, T. M. N. Bui, T. Q. Dinh, E. Hosseinzadeh, T. F. Yu, and J. Marco, "Remaining energy estimation for lithium-ion batteries via Gaussian mixture and Markov models for future load prediction," *J. Energy Storage*, vol. 28, Apr. 2020, Art. no. 101271, doi: 10.1016/j.est.2020.101271.
[55] F. Yang, D. Wang, Y. Zhao, K.-L. Tsui, and S. J. Bae, "A study of the relationship between Coulombic efficiency and capacity degradation of commercial lithium-ion batteries," *Energy*, vol. 145, pp. 486–495, Feb. 2018, doi: 10.1016/j.energy.2017.12.144.
[56] C. C. Tan, M. Walker, G. Remy, N. Kourra, F. Maddar, S. Dixon, M. Williams, and M. J. Loveridge, "Ageing analysis and asymmetric stress considerations for small format cylindrical cells for wearable electronic devices," *J. Power Sources*, vol. 472, Oct. 2020, Art. no. 228626, doi: 10.1016/j.jpowsour.2020.228626.
[57] S. Atalay, M. Sheikh, A. Mariani, Y. Merla, E. Bower, and W. D. Widanage, "Theory of battery ageing in a lithium-ion battery: Capacity fade, nonlinear ageing and lifetime prediction," *J. Power Sources*, vol. 478, Dec. 2020, Art. no. 229026, doi: 10.1016/j.jpowsour.2020.229026.
[58] X. Han, L. Lu, Y. Zheng, X. Feng, Z. Li, J. Li, and M. Ouyang, "A review on the key issues of the lithium ion battery degradation among the whole life cycle," *eTransportation*, vol. 1, Aug. 2019, Art. no. 100005, doi: 10.1016/J.ETRAN.2019.100005.
[59] J. Jaguemont, A. Nikolian, N. Omar, S. Goutam, J. Van Mierlo, and P. Van den Bossche, "Development of a two-dimensional-thermal model of three battery chemistries," *IEEE Trans. Energy Convers.*, vol. 32, no. 4, pp. 1447–1455, Dec. 2017, doi: 10.1109/TEC.2017.2697944.
[60] J. Ferreira and J. Ferreira, "An experiment to assess bit error rate in CAN," in *Proc. 3rd Int. Workshop Real-Time Netw. (RTN)*, 2004, pp. 15–18.
[61] P. V. Chombo and Y. Laoonual, "A review of safety strategies of a li-ion battery," *J. Power Sources*, vol. 478, Dec. 2020, Art. no. 228649, doi: 10.1016/j.jpowsour.2020.228649.
[62] D. P. Finegan, J. Darst, W. Walker, Q. Li, C. Yang, R. Jervis, T. M. M. Heenan, J. Hack, J. C. Thomas, A. Rack, D. J. L. Brett, P. R. Shearing, M. Keyser, and E. Darcy, "Modelling and experiments to identify high-risk failure scenarios for testing the safety of lithium-ion cells," *J. Power Sources*, vol. 417, pp. 29–41, Mar. 2019, doi: 10.1016/j.jpowsour.2019.01.077.

TIMOTHY A. VINCENT received the degree (Hons.) and the Ph.D. degree in electronic engineering from the School of Engineering, University of Warwick, Coventry, U.K., in 2013 and 2017, respectively.

He currently works as an Assistant Professor at WMG, University of Warwick. His research interests include miniature sensors, communication networks for vehicular applications, and instrumenting smart cells.

BEGUM GULSOY received the M.Sc. degree in sustainable energy technologies from the School of Engineering, University of Warwick, Coventry, U.K., in 2020. She is currently a Project Engineer at WMG, University of Warwick, and has experience in battery characterization, electrochemical battery testing, and *in-situ* battery monitoring systems. Her current research is focused on developing *in-situ* thermal and pressure monitoring systems for smart battery applications.

JONATHAN E. H. SANSOM received the 2:1 Honors degree in life sciences (with chemistry) from The Open University, in 1999, and the Ph.D. degree in solid state chemistry from the University of Surrey, in 2003, developing novel electrolyte materials for solid oxide fuel cells. During this period of study, he was also working with British Telecom, engaged with analogue to digital transmission upgrade activities. On completion of his Ph.D., he spent a period of time at the University of Surrey developing novel cathode materials for solid oxide fuel cells before taking up a position with a commercial fuel cell company developing and scaling up alkaline fuel cells. He is currently a Lead Engineer and part of the Cell Instrumentation Team at WMG, University of Warwick, Coventry, U.K.

JAMES MARCO received the D.Eng. degree from the University of Warwick, in 2000. He is currently employed at the University of Warwick as a Professor in battery systems engineering, where he leads a research group focused on battery characterization, modeling, and control. His research interests include the challenge of scaling-up individual battery cells to complete energy storage systems. Example areas include model, control and experimental design to quantify electro-thermal heterogeneity at cell and system level, and methods to extend battery useful life through repurposing and re-use.